

# Tectonics

## RESEARCH ARTICLE

10.1029/2020TC006516

### Key Points:

- The Isua supracrustal belt (ISB) records three tectono-metamorphic events
- Petrographic observations and geothermobarometry show no clear metamorphic gradients in the ISB
- Syn-tectonic metamorphic records are consistent with heat-pipe model predictions for the evolution of the belt

### Supporting Information:

- Supporting Information S1

### Correspondence to:

A. Ramirez-Salazar,  
[cears@leeds.ac.uk](mailto:cears@leeds.ac.uk)

### Citation:

Ramirez-Salazar, A., Müller, T., Piazzolo, S., Webb, A. A. G., Hauenberger, C., Zuo, J., et al. (2021). Tectonics of the Isua supracrustal belt 1: P-T-X-d constraints of a polymetamorphic terrane. *Tectonics*, 40, e2020TC006516. <https://doi.org/10.1029/2020TC006516>

Received 11 SEP 2020

Accepted 5 DEC 2020

© 2021. The Authors.

This is an open access article under the terms of the [Creative Commons Attribution License](https://creativecommons.org/licenses/by/4.0/), which permits use, distribution and reproduction in any medium, provided the original work is properly cited.

## Tectonics of the Isua Supracrustal Belt 1: P-T-X-d Constraints of a Poly-Metamorphic Terrane

Anthony Ramirez-Salazar<sup>1</sup> , Thomas Müller<sup>1,2</sup> , Sandra Piazzolo<sup>1</sup> ,  
 A. Alexander G. Webb<sup>3</sup> , Christoph Hauenberger<sup>4</sup>, Jiawei Zuo<sup>3</sup> , Peter Hapfrock<sup>5</sup> ,  
 Jason Harvey<sup>1</sup> , Tsz Kin Wong<sup>3</sup>, and Callum Charlton<sup>1</sup>

<sup>1</sup>School of Earth and Environment, University of Leeds, Leeds, UK, <sup>2</sup>Geowissenschaftliches Zentrum, Georg-August-Universität Göttingen, Goldschmidtstrasse 1, Göttingen, Germany, <sup>3</sup>Division of Earth and Planetary Science and Laboratory for Space Research, University of Hong Kong, Hong Kong, China, <sup>4</sup>Department of Earth Sciences, University of Graz, Universitätsplatz 2, Graz, Austria, <sup>5</sup>Department of Earth and Ocean Sciences, University of North Carolina Wilmington, Wilmington, NC, USA

**Abstract** The Eoarchean Isua supracrustal belt (ISB) has been interpreted as one of the earliest records of subduction processes, leading to the conclusion that a plate tectonic geodynamic system was likely operating since the early Archean. However, proposed tectonic models remain difficult to evaluate as our understanding of the metamorphic and structural evolution remains fragmentary. Here, we present a metamorphic study of the supracrustal rocks of the ISB. We used petrographic and microstructural observations, phase equilibria, isopleth geothermobarometry, and conventional thermometry to explore the prograde, peak, and retrograde metamorphic evolution of the northeastern ISB. Our results show that the ISB records a syn-tectonic, amphibolite facies metamorphic event ( $M_1$ ) with peak conditions of 550°C–600°C and 0.5–0.7 GPa.  $M_1$  was followed by a static, lower amphibolite facies metamorphic event ( $M_2$ ; <540°C and <0.5 GPa). Published constraints suggest that  $M_1$  and  $M_2$  occurred in the late Eoarchean (>3.5 Ga) and the Neoarchean (<2.9 Ga), respectively. These events are partially overprinted by late low temperature (<500°C) retrogression ( $M_3$ ) that is most intensely developed in the northeastern part of the belt; it typically overprints some peak mineral phases while preserving the peak fabric. Our findings are consistent with spatially homogeneous syn-tectonic amphibolite facies metamorphism and macroscale folding. Such features are predicted by a heat-pipe tectonic model. Therefore, our findings permit the interpretation of the ISB as a record of early nonuniformitarian tectonic processes.

### 1. Introduction

Models to describe the nature of the Earth's crustal evolution during the Archean vary substantially, from horizontal lithospheric motions with subduction-like movement (Abbott et al., 1994), to vertical tectonics defined by sub-/intra-lithospheric diapirism (Collins, 1989; Sizova et al., 2015), extensive volcanism (Moore & Webb, 2013; Turcotte, 1989), and the formation of a single-plate lithosphere. First-order questions include when and how horizontal lithospheric motion (e.g., subduction) became the dominant process by which Earth's interior cools, deforms, and evolves (Lenardic, 2018). A change in geodynamics between ~3.2–2.5 Ga is proposed based on the global geochemical and zircon record indicating an increased contribution of reworked crust for magma generation while juvenile mantle additions decreased during that time (e.g., Dhuime et al., 2012; Moyen & Laurent, 2018). A recent review of the existing metamorphic record suggests that Earth has experienced spatial and temporal changes of global crustal thermal gradients probably linked to transitions in the tectonic regime, from stagnant-lid tectonics to mobile-lid plate tectonics (Brown & Johnson, 2018). The main changes occurred at ~2.5 Ga, ~1.0 Ga, and 0.72 Ga, Ga which are associated with the widespread appearance of paired metamorphic belts, dominance of high T/P gradients (>775°C/GPa), and increasing abundance of low T/P gradients (<375°C/GPa), respectively. The presence of a distinct bimodality of low and high T/P gradients is indeed a feature commonly associated with plate tectonics (Brown, 2010; Miyashiro, 1961, 1973) and its gradual emergence argues for progressive onset and evolution to horizontal-dominated geodynamics since the Neoarchean (Holder et al., 2019). In stark contrast with these interpretations, multiple subduction-driven events are invoked to explain the origin and evolution of the Eoarchean Isua supracrustal belt (ISB) of southwest Greenland (Figure 1), one of the oldest metamorphic terranes known, which some workers have interpreted to reflect the onset of plate tectonics as

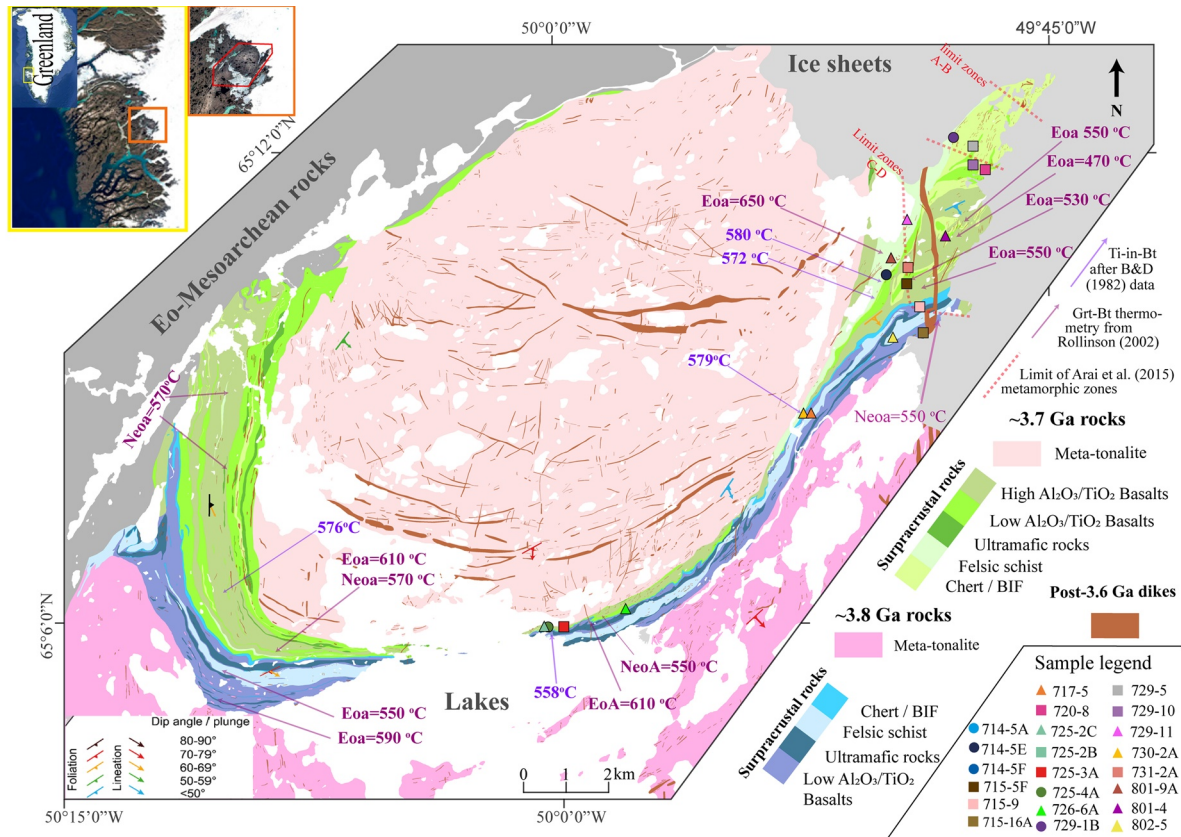


**Figure 1.** Geological map of the Isua Supracrustal Belt showing the location of samples used in this study, modified from Zuo et al. (2021) and Nutman and Friend (2009). Garnet-biotite temperatures from Rollinson (2002) are divided into Eoa = Eoarchean and Neoa = Neoproterozoic metamorphic events, according to the interpretations of the author. Color and symbol coding of the samples follows the rest of the figures, symbol coding represent the interpreted protolith: triangles: felsic metavolcanic rocks; squares: metamafic rocks (amphibolites and mafic schists); and circles: metasedimentary rocks (metapelites and BIFs). Samples that share locality/outcrop: 714-5A, 714-5E and 714-5F; 725-2c and 725-2b; 729-1B and 729-1A.

early as 3.6–3.8 Ga (Komiya et al., 1999; Nutman & Friend, 2009; Nutman et al., 2015). Structural studies of the belt (Webb et al., 2020) together with new geochemical data of the adjacent Eoarchean tonalite-trondhjemite-granodiorite (TTG) bodies (Gardiner et al., 2019) challenge the unequivocal interpretation that the ISB was generated in a horizontal tectonics regime and alternatively suggest that a vertical tectonic scenario is equally plausible. Despite the importance of the metamorphic evolution in deciphering the geodynamic setting of an area (e.g., Brown, 1993; Brown & Johnson, 2018; Miyashiro, 1961), studies of the metamorphic evolution of the ISB are relatively scarce (e.g., Appel et al., 2001; Arai et al., 2015; Blichert-Toft & Frei, 2001; Boak & Dymek, 1982; Dymek et al., 1988; Frei et al., 2002; Gauthiez-Putallaz et al., 2020; Hayashi et al., 2000; Heijlen et al., 2006; Komiya et al., 2002; Nutman et al., 2020; Rollinson, 2002, 2003), and existing studies present results with contrasting distributions of the P-T peak conditions across the belt and conflicting P-T evolutions.

In this contribution, we present a systematic analysis of the P-T-X-d-(t) evolution of the ISB, linking metamorphic data to structural data at the micro to macro scale. In-depth petrographic observations combined with classic and phase equilibria geothermobarometry provide an extended data set that allows us to identify the number of metamorphic events, their respective peak conditions recorded in the belt, and their spatial distribution. We present our results alongside a companion study on the microstructures and strain distribution recorded in the syn-tectonic fabrics of quartz-rich lithologies, centered on strain and shear sense analyses (Zuo et al., 2021). The data set presented here enables us to discuss in depth the metamorphic spatial and temporal evolution of the belt in terms of endmember tectonic models and hence implications for Archean geodynamics.

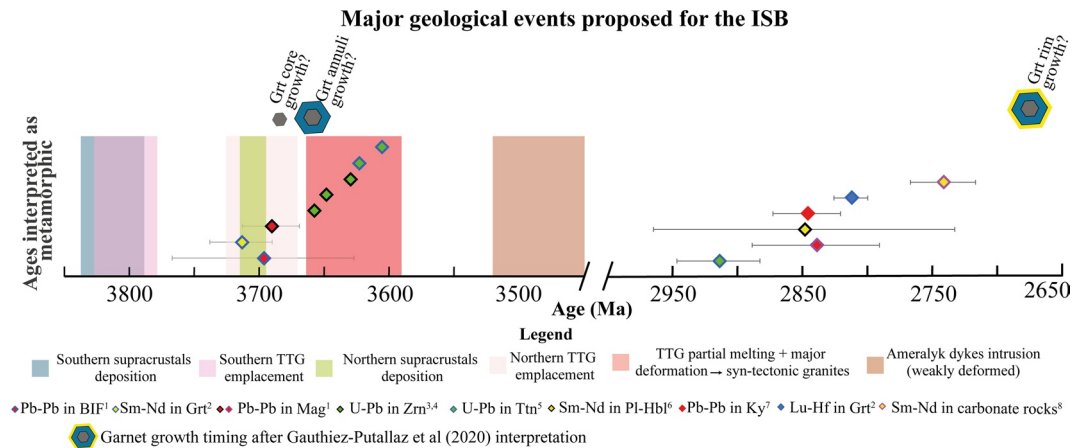


**Figure 2.** Timeline showing the major geological events interpreted for the ISB (bands) and ages interpreted as metamorphic (motifs with error bars). Interpretation of the garnet growth from Gauthiez-Putallaz et al. (2020). Geochronological data from Nutman and Friend (2009). Metamorphic ages references: 1. Frei et al. (1999); 2. Blichert-Toft and Frei (2001); 3. Nutman et al. (2013); 4. Crowley (2003); 5. Crowley et al. (2002); 6. Gruau et al. (1996); 7. Rosing and Frei (1999); 8. Shimizu et al. (1990). ISB, Isua supracrustal belt.

## 2. Geological Setting, Previous Work, and Interpretations

The ~35-km-long, arcuate ISB (Figure 1) is part of the North Atlantic craton (Bridgwater et al., 1973) and is located in southwest Greenland as part of the northern part of the Itsaq Gneiss Complex (Nutman et al., 1996). The ISB comprises a series of felsic and mafic metavolcanic rocks exhibiting arc-like geochemistry (e.g., Polat et al., 2002) intercalated with cherts, banded iron formations (BIFs), clastic metasedimentary rocks, and minor ultramafic metaigneous rocks (Nutman et al., 1984). The ISB is flanked by 2 km-scale TTG bodies with distinct crystallization ages of 3.8 and 3.7 Ga (Figure 2). Analysis of a large U-Pb zircon data set revealed that the supracrustal rocks can be subgrouped in two distinct metavolcanosedimentary units of 3.8 and 3.7 Ga age, separated by a <1 km-thick, c. 3.75 Ga discontinuous metasedimentary sequence of chert, BIFs, and carbonates known as the “dividing sedimentary unit” (Nutman & Friend, 2009). Field observations of the ISB suggest that each subunit is exclusively in contact with the similar-aged TTG. In addition, some deformed 3.66–3.6 Ga granitic intrusions (Nutman & Friend, 2009) and the weakly deformed, c. 3.5 Ga Ameralik dykes cross-cut both the 3.8 and 3.7 Ga supracrustal rocks and the TTGs (Nutman et al., 2004) suggesting a shared history since at least 3.66 Ga.

Parts of the ISB show primary igneous and sedimentary structures including pillow basalts (Nutman et al., 1996), graded bedding (Nutman, 1984), cross lamination (Nutman et al., 2017), and relic stromatolites (Nutman et al., 2016); these have been interpreted to mark areas of low deformation (e.g., Nutman et al., 2016). However, the existence of some of these structures and the differential intensity of their deformation have recently been questioned (Allwood et al., 2018; Webb et al., 2020), suggesting that most of the exposed rocks show signs of deformation and metamorphism that clearly modified the primary structures. In the literature, multiple metamorphic events have been documented in the ISB, some of which are only locally reported (e.g., low-grade sea-floor hydrothermal metamorphism; Appel et al., 2001), with broadly two major medium- to high-temperature episodes recognized and documented to have affected the entire belt. These events are typically placed in the Eoarchean and Neoproterozoic based on several isotopic ages that are interpreted to reflect the metamorphic age of the events (Figure 2; Blichert-Toft & Frei, 2001; Crowley et al., 2002; Crowley, 2003; Frei et al., 1999; Gruau et al., 1996; Nutman et al., 2013; Rosing & Frei, 1999; Shimizu et al., 1990). The most pervasive metamorphic event is syntectonic to the penetrative foliations, that are parallel to the belt margins, and steep southeast-plunging lineation (Figure 1; e.g., Webb et al., 2020) that are characteristic of the Isua rocks (e.g., Boak & Dymek, 1982). For this event, the weakly deformed Ameralik dykes cross-cutting the belt provide a minimum age of c. 3.5 Ga (Nutman et al., 2004). The younger event is recognized in posttectonic garnet rims (Blichert-Toft & Frei, 2001; Rollinson, 2002, 2003) and non-foliated lower amphibolite metamorphic paragenesis in the Ameralik dykes (Nutman et al., 2004). Additionally, detailed investigations of the textures and chemical composition of garnets across the belt revealed

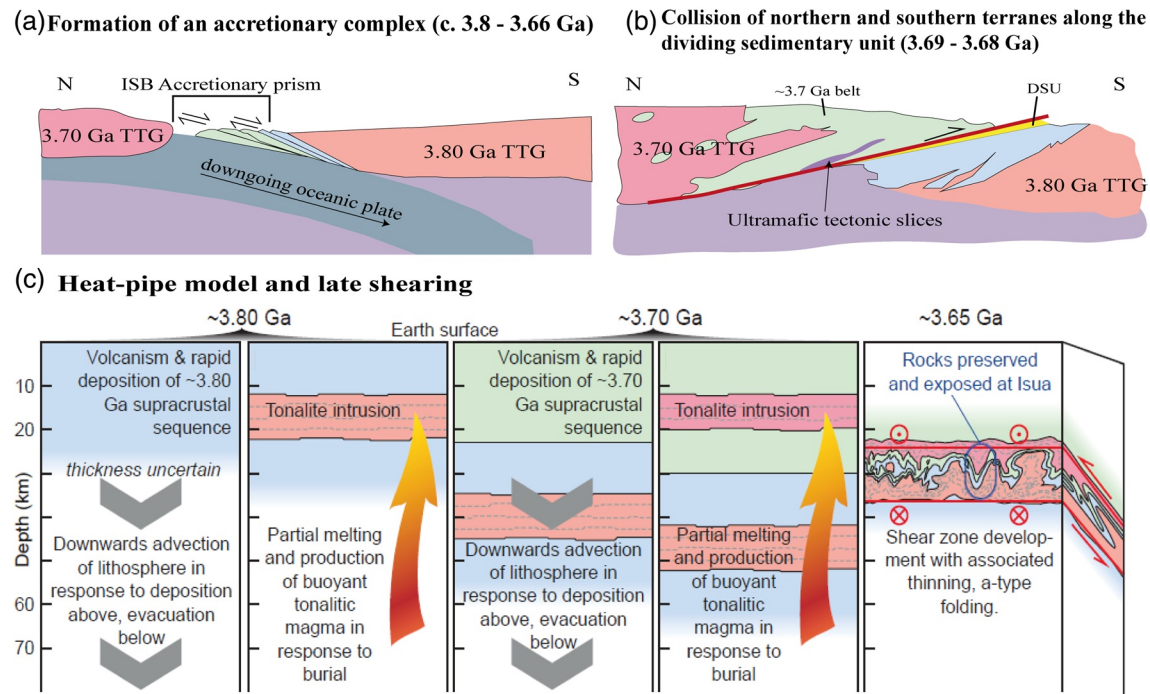


**Figure 3.** Tectonic model proposed for the evolution of the ISB. (a) South-dipping accretionary complex model (modified from Arai et al., 2015) (b) North-dipping subduction-collision model (modified from Nutman & Friend, 2009); (b and c) heat-pipe model (modified from Webb et al., 2020). ISB, Isua supracrustal belt.

the common appearance of three to four distinct zones (core-annuli-rim) within individual grains (Gauthiez-Putallaz et al., 2020; Rollinson, 2002, 2003), leading to the interpretation that the core could represent an earlier medium-temperature metamorphic episode preceding the large syn-tectonic event (Figure 2) responsible for most of the deformation (Gauthiez-Putallaz et al., 2020; Rollinson, 2002).

### 2.1. Tectonic Models for the Eoarchean Evolution of the ISB and Their Relationship With the Metamorphic Record

The tectonic scenario responsible for the Eoarchean tectono-metamorphic event during which the most pervasive mineral, microstructural, and deformational features of Isua developed is still debated. Three main models have been proposed (Figure 3): two models proffer uniformitarian plate tectonic interpretations (e.g., Arai et al., 2015; Komiya et al., 1999; Nutman & Friend, 2009; Nutman et al., 2013, 2020), and a third model suggests that heat-pipe tectonics could explain the geological record of Isua (Webb et al., 2020).

Both plate tectonic models predict systematic metamorphic patterns across the area. The first plate tectonic model suggests that the ISB represents an accretionary complex characterized by southeast-directed duplex structures in the supracrustal rocks (Komiya et al., 1999), which developed during the subduction of the oceanic plate attached to the 3.7 Ga TTG under the  $\approx$ 3.80 TTG (Figure 3a, Arai et al., 2015; Komiya et al., 1999). This model anticipates a metamorphic gradient with increasing P-T conditions from north to south across the northeastern portion of the belt (Arai et al., 2015; Hayashi et al., 2000; Komiya et al., 2002). This is consistent with a suggested northeast-southwest increase in PT conditions based on mineral composition and phase equilibria geothermobarometry from the end of the northeastern belt to the central part of it from 0.3 GPa and 380°C to 1.1 GPa and 800°C (Figure 1; Arai et al., 2015).

The second plate tectonics model argues for orogenic crustal thickening in response to collision of two proto-arcs, with subsequent orogenic collapse via development of an extensional core complex (Nutman et al., 2013). In this model, north-dipping subduction of the 3.8 Ga belt under the 3.7 Ga belt drives the collision with the dividing sedimentary unit acting as the tectonic boundary (Nutman & Friend, 2009) (Figure 3b). Syn-deformational Barrovian-type metamorphism is predicted for this model, with P-T conditions

increasing continuously from the 3.8 Ga belt to the 3.7 Ga TTG (Nutman et al., 2013). The reported early metamorphic event recorded in garnet cores of the 3.7 Ga sequence has been interpreted in support of this model, attributed to the amalgamation phase of the proto-arc (Gauthiez-Putallaz et al., 2020; Nutman et al., 2015). Based on the report of kyanite in metapelites of the 3.7 Ga belt and garnet-clinopyroxene-hornblende-quartz-plagioclase assemblages in the center of the 3.7 Ga TTG, Nutman et al. (2013) interprets an increase in PT conditions, from greenschist/lower amphibolite facies in the 3.8 Ga belt to amphibolite facies in the 3.7 Ga belt and up to high-pressure granulite facies in the center of the 3.7 Ga TTG. The authors then argue that this interpretation is consistent with subduction type tectonic model. In addition, a metamorphic record typical for paired metamorphic belts characteristic of convergence tectonics in young metamorphic belts (Brown, 2010; Miyashiro, 1961, 1973) is expected for this second model, with low T/P gradients developing in the subducting plate and high T/P gradients in the upper plate (Nutman et al., 2020). Nutman et al. (2020) argue using phase equilibria diagrams from a mid-ocean ridge basaltic protolith and zircon-TTG trace element chemistry, that there is indeed a paired metamorphism preserved in Isua and the Itsaq Gneiss Complex. In their interpretation, cold T/P gradients ( $<500^{\circ}\text{C}/\text{GPa}$ ) are recorded in the high-pressure garnet-granulites and in the garnet/rutile chemical signature of the TTGs, which may represent partial melting of garnet-rutile eclogites. In contrast, hot T/P conditions ( $>1000^{\circ}\text{C}/\text{GPa}$ ) would be represented by TTGs with no signature of residual garnet and in equilibrium with orthopyroxene-granulites (Nutman et al., 2020). Nutman et al. (2020) suggest even colder gradients ( $<200^{\circ}\text{C}/\text{GPa}$ ) due to the interpretation of ultra-high pressure (UHP) metamorphism on the basis of the presence of F bearing Ti-chondrodite/clinohumites in some ilmenite-carbonate dunites. However, it is important to bear in mind, that halogens, ilmenite and  $\text{CO}_2$  have been shown to stabilize Ti-chondrodite/humite to higher temperatures and lower pressures in other settings (cf. Ehlers & Hoinkes, 1987; Shen et al., 2015), thus questioning these rocks to unequivocally represent UHP conditions.

The heat-pipe model suggests that the ISB was emplaced via rapid volcanic resurfacing, depositing first the rocks from the 3.8 Ga belt and then the younger lithologies in straight stratigraphic sequence (Webb et al., 2020). Intervals of rapid deposition led to burial, static metamorphism, and melting of deeply buried hydrated mafic crust to form TTGs. Subsequently, a tectono-metamorphic episode produced amphibolite-facies syn-tectonic metamorphism and structural thinning across the whole belt in response to either (a) heat-pipe contraction (global lithospheric subsidence on a spherical body forces contraction) or (b) a plate-breaking event representing transition to plate tectonics. Within this shear zone an A-type fold developed (Webb et al., 2020) with randomly distributed opposite shear senses (Zuo et al., 2021). Any early record of burial metamorphism should record increasing pressure conditions from the top to the bottom of the sequence, that is, from 3.7 Ga rocks to 3.8 Ga rocks. For the subsequent thinning and syn-tectonic metamorphic period, the model anticipates nearly homogenous amphibolite facies metamorphism (Figure 3c), in stark contrast to the metamorphic gradients predicted in plate tectonic models. To date, the heat pipe model is consistent with the apparent lack of metamorphic gradient interpreted from the amphibolite facies temperatures ( $550^{\circ}\text{C}$ – $650^{\circ}\text{C}$ ) returned from garnet-biotite thermometry (Boak & Dymek, 1982; Rollinson, 2002, 2003) that show no clear spatial variations (Figure 1). The heat-pipe model is further supported by geochemical data identifying the TTGs as a likely product of the hydrated tholeiites from the ISB (Gardiner et al., 2019; Hoffmann et al., 2014, 2019; Nagel et al., 2012) and metasediments (Gauthiez-Putallaz et al., 2020) in a thickened/buried crust (Gardiner, 2019; Hoffmann, 2014, 2019; Nagel et al., 2012; Smit et al., 2019).

### 3. Results

#### 3.1. Petrography

For this study, we selected samples based on (1) their spatial distribution, trying to cover transects along north-south and east-west directions in the eastern arm of the belt as well as samples from both the 3.7 Ga and the 3.8 Ga sequences (Figure 1), and (2) their potential to provide geothermobarometric information (e.g., presence of important geothermometers such as garnet and biotite). The selection aimed to characterize the mineralogical changes along the belt and quantify the P-T peak distribution to test the presence or absence of metamorphic gradients. We conducted a detailed study on 23 samples, most of which are garnet bearing, from three main lithologies namely felsic metavolcanics, amphibolites, and metapelites with minor

mafic schists and BIFs. In the field, the rocks are characterized by a distinct foliation and lineation. Samples were cut parallel to lineation and perpendicular to foliation. Below we present a summary of the mineralogical and microstructural observations of the different samples (Table 1).

Nine samples of felsic metavolcanics (Table 1, 717-5, 725-2c, 726-6A, 729-1A, 729-11, 730-2A, 801-4, 801-9A, 802-5) show peak mineral assemblages of quartz + biotite + plagioclase + garnet<sub>syn</sub> ± muscovite ± tourmaline ± epidote/clinozoisite ± ilmenite ± calcite ± K-feldspar ± apatite ± titanite. These samples typically exhibit a strong foliation with lepidoblastic layers intercalated with quartz-rich granoblastic layers that are deflected by large garnet poikiloblasts/clusters, typically developing pressure shadows (Figures 4a and 4b; Figure S1a, in the supportive information) and occasional garnet boudin structures in some samples (725-2c and 726-6A). Different garnet microstructures can be identified in this lithology (Figure 4; Figure S1). Garnet within sample 729-11, located in the north-central part of the 3.7 Ga belt (Figure 1), shows up to three zones: (i) core with relatively small, mainly quartz, inclusions (<20 μm) without a clear internal foliation pattern, followed by (ii) annulus of larger inclusions (20–50 μm) with spiral-like internal foliation pattern, and (iii) an inclusion-poor rim with euhedral facets cutting the external foliation (Figure 3b). Garnets of samples 725-2c (Figure S1b) and 801-9A (Figure S1c) from the 3.7 Ga belt show garnets with a clear inclusion-rich core and an inclusion-poor rim whereas garnets from samples 717-5, 726-6A, 730-2A, and 802-5 from the 3.8 Ga belt and sample 801-4 from 3.7 Ga belt exhibit clusters of skeletal-like microstructures (Figure S1), some of which contain small euhedral garnets that overgrow the foliation (Figure 3a). The quartz trails in the cluster/porphyroblast from samples 802-5 and 717-5 (Figure S1a) show arc-like shapes converging in the pressure shadows, whereas in sample 726-6A (Figure S1e), the trails are parallel to the external foliation at the pressure shadows, but oblique at the body of the sigmoidal garnet/cluster. Sample 17725-2c contains well-developed S-C fabric structures in the external foliation. Late retrogression at upper greenschist/lower amphibolite facies conditions is commonly observed in the felsic rocks. For example, sample 717-5 displays micro-shear zones that overprint the peak assemblages, where muscovite grows along observed fractures (Figure S2a) that cross-cut the whole rock. Replacement of biotite by chlorite, mimicking the penetrative external foliation, is common in the rest of the samples as well as sericitization of plagioclase.

The peak assemblage of the eight amphibolites (Table 1, 715-5F, 715-9, 715-9, 720-8, 725-2b, 725-3a, 729-10, 731-2A) comprises amphibole + biotite + quartz ± garnet<sub>syn</sub> ± plagioclase + epidote/clinozoisite ± ilmenite ± calcite ± muscovite. These rocks are foliated amphibolites typically containing garnet poikiloblasts, and minor amphibole porphyroblasts that deflect the external foliation. Sample 731-2A also shows boudinage structures (Figure 4c). Garnets commonly contain inclusion-rich cores, with different inclusion patterns observed in various samples (Figure S1; see Table 1). The inclusions in the garnet core of sample 720-8 are randomly oriented (Figure S1f), whereas in samples 715-5F, 715-9, and 731-2A, the internal foliation in the ellipsoidal large garnets (typically >1 cm) displays arc-like patterns that converge toward the pressure shadows and continue into the external foliation (Figure 4c). In sample 725-3a, garnets occur as complex aggregates of large grains (>0.4 cm) with weakly curved inclusion patterns, discontinuous with the external foliation (Figures S1f and S1g). The amphibolites show various post-tectonic upper greenschist-lower amphibolite facies features: (1) most of the garnets display inclusion-poor euhedral rims overgrowing the external foliation (Figure S1f); (2) in sample 715-9, a vein dominated by post-tectonic calcite cross-cuts one of the garnets perpendicularly to the internal foliation, and euhedral garnet crystals grow toward the center of the vein (Figure 5a); (3) in sample 720-8, calcite veins cross-cut the main external foliation at ~30° and are overprinted by garnet growth (Figure 5b); (3) epidote grains, typically associated with muscovite and ilmenite, overprint amphibole (sample 725-3A; Figure S2c) and grow in garnet fractures with no preferred shape or crystallographic orientation; and (4) randomly oriented biotite grains, and quartz-calcite crystals with a granoblastic texture replace garnets (sample 720-8) (Figure 5c). Late (upper) greenschist facies replacement microstructures overprinting the syn-tectonic and post-tectonic medium temperature assemblages are commonly observed. They are characterized by epidotization of plagioclase, and mainly chlorite (sometimes associated with calcite), either randomly overgrowing peak minerals (Figure 5d) or mimicking the foliation by replacing biotite (Figure 5e).

Two metapelitic samples (714-5E and 714-5F) collected less than <10 m apart in the same outcrop reveal peak assemblages of quartz + garnet<sub>syn</sub> + muscovite + chlorite + tourmaline + sulfides ± staurolite. The rocks show lepidoblastic foliation and elongated quartz grains that are deflected by large garnet por-

**Table 1**  
Mineral Relationships and Data Collected for Each Sample

Sample ID	Metafelsic rocks	Lithology	Age (Ga)	Inclusions in garnet	Syn-tectonic paragenesis (M <sub>1</sub> )	Post-tectonic paragenesis (M <sub>2</sub> )	Low-T paragenesis (M <sub>3</sub> )	P-T-X data				GPS coordinates	
								M.C	Grt-Bt	TiB	P.S.	Longitude	Latitude
717-5	Mfv	3.8	Qz, Bt, Ms, minor Ap, Cal, Tur, Aln, Zrn	Qz + Bt + Pl + Ms + Czo + Grt + Kfs minor Cal + Tur + Ilm	-	Ms, Sericitization	X	X	-	X	65.152608	-49.84904	
725-2c	Mfv	3.7	Qz, Bt, Ilm	Qz + Bt + Pl + Grt + Ilm + minor Tur	Grt + Ilm	-	X	X	X	65.098302	-50.00803		
726-6A	Mfv	3.75	Qz, Bt, Pl, Ms, Ilm	Qz + Bt + Ilm + Grt + Pl + Ms Minor Ap + Hm + Cal	-	Chl	X	X	-	65.101806	-49.967241		
JZ17729-1A	Mfv	3.7	Qz, Bt, Ms, Pl	Qz + Grt + Pl + Ms + Chl (?) + Ilm	-	Chl	X	-	-	65.111243	-50.017674		
729-11	Mfv/Mmp	3.7	Qz, Ap, Ilm, Aln	Qz + Bt + Ms + Pl + Grt + Tur + Ap + Ilm	Grt	Chl	-	-	-	65.183238	-49.82114		
730-2A	Mfv	3.75	Qz, Ilm, Cal, Bt	Bt + Qz + Pl + Grt + Czo + Ilm + Ms + minor Tur + Cal + Ap	Grt + Czo	-	X	X	-	65.142622	-49.87623		
801-9A	Mfv	3.7	Qz, Bt, Ilm	Qz + Bt + Plg + Grt + Cal + minor Ep/Czo + Ilm	Grt	Chl + Ms	X	X	-	65.18258	-49.80878		
JZ17801-4	Carbonated -Mfv	3.7	Qz, Bt, An	Qz + Grt + Bt + Ms + Ep + Pl minor Ttn + Ap + Cal	Grt	-	X	-	-	65.179341	-49.803351		
802-5	Mfv	3.8	Qz, Cal, Ms, Tur, Ilm, Bt, Ep	Qz + Ms + Bt + Pl + Tur + Grt + Ep + Opaq	Grt + Cal	Sericitization	-	-	-	65.158051	-49.831399		
715-9	Am	3.8	Qz, Ap, Chl, Bt, Cal, An, Ilm, Wo	Qz + Bt + Grt + Pl + Amp + Ep minor Ilm	Grt + Cal	Chl, Cal veins	X	X	-	65.16436	-49.81711		
JZ17715-5F	Am	3.7	Qz, Cal, Bt, Ap, Amp, Hm	Qz + Bt + Grt + Cal minor Ap + Amp	-	Chl, Qz + Cal veins	-	-	-	65.169422	-49.823217		
JZ17715-16A	Am	3.8	Act, Ep, An, Cal, Bt, Qz, Ap	Qz + Bt + Grt + Amp + An + Ab + Cal minor Act + Ttn + Ap	-	-	X	X	-	65.158913	-49.815456		
720-8	Mafic schist	3.7	Cal, Qz, Ilm, Ap	Qz + Bt + Amp + Cal + Grt + Czo + Ilm	Qz + Grt + Czo + Ilm	Cal	X	-	X	65.193078	-49.782867		
725-3a	Am	3.7	Qz, Ilm, Czo	Amp + Pl + Qz + Bt + Grt + Ilm	Grt + Czo + Ms + minor Cal	Chl + Czo	X	-	-	65.098261	-49.998603		
725-2b	Amp	3.7	-	Act + Mg-Hbl + Chl	-	Chl + Tre + Cal	X	-	-	65.098302	-50.00803		

**Table 1**  
*Continued*

Sample ID	Lithology	Age (Ga)	Inclusions in garnet	Syn-tectonic paragenesis (M <sub>1</sub> )	Post-tectonic paragenesis (M <sub>2</sub> )	Low-T paragenesis (M <sub>3</sub> )	P-T-X data				GPS coordinates	
							M.C	Grt-Bt	TiB	P.S.	Longitude	Latitude
729-5	Mafic schist	3.7	Qz	Bt	Grt (?)+ Ilm	Chl	-	-	-	-	65.1198128	-49.788794
729-10	Mafic schist	3.7	-	Amp + Bt + Qz + Ilm (maybe Cal)	-	Cal + Chl	X	-	X	-	65.1194247	-49.788856
731-2A	Amp	3.7	Qz, Ilm, Ms, Ep/ Czo, Alm, Bt, minor Cal and Chl	Grt + Amp + Bt + Qz + Czo + Zo + Ms + Ilm + minor Cal	Grt	-	-	-	X	X	65.1173048	-49.822507
Metasedimentary rocks	Mmp	3.7	Qz, Bt, Po, minor Cal and Amp	Qz + Bt + Amp + Grt + Pl + Ilm	Grt	Chl + Act	X	X	X	X	65.171295	-49.833468
714-5E	Mp	3.7	Qz, Ms, Cld, Chl, Ilm, Tur, small Plg	Qz + Grt + Ms + Cld + Chl + Tur + Pyr	Grt	Chl + Ms	X	-	-	X	65.171295	-49.833468
714-5F	Mp	3.7	Qz, Ms, Cld, Chl, Ilm, Tur	Qz + Grt + Chl + Ms + Tur + St + Pyr	Grt	Ms + Chl	-	-	-	X	65.171295	-49.833468
725-4A	Chert	3.7	Bt, Qz, Ap, Zrn and minor Hbl	Hbl + Bt + Qz + Grt + Czo + Pl + minor Ilm	Grt	-	X	X	-	-	65.09825	-50.0062
729-1B	Mmp	3.7	Qz, Ilm, Ms, Ep/Czo, Bt, minor Cal and Chl	Qz + Bt + Amp + Grt + Pl + Ilm + minor Cal + early C(z)	Grt <sub>2</sub>	Chl + Czo(?)	X	-	X	X	65.20005	-49.798507

Notes. Mineral abbreviations as in Whitney and Evans (2010). OB = Outer-belt; IB = inner-belt; M.C. = Mineral chemistry; Grt-Bt = Garnet-Biotite thermometry; TiB = Ti-in-Biotite thermometry; P.S. = Phase equilibria thermobarometry. Lithology: Mfv = Metafelsic volcanics; Am = Amphibolite; Mp = Metapelite; Mmp = "mafic" metapelite. Most samples ID prefix is TM17-, (e.g., 714-5A = TM17714-5A), apart from those with JZ, which in case sample ID prefix is JZ17- (see Supporting Information for details on the sample nomenclature).

phyroblasts ( $\approx 1$  cm). Garnets display spiral-like inclusions patterns from the core to the annulus that are overgrown by an inclusion-poor rim (Figures 4e and 4f), which typically shows euhedral facets and overgrows the foliation (Figures 4e and 5f). The size of the inclusions in the trails is smaller in the core ( $< 100 \mu\text{m}$ ) and larger toward the annulus ( $> 200 \mu\text{m}$ , Figures 4e and 4f). Staurolite crystals, typically overprinted by muscovite (Figure S2d), appear in the matrix of sample 714-5F, in contrast to chloritoid, which only occurs as inclusions in the garnets, occasionally growing in contact with muscovite along irregular borders (Figure 4f). In these samples, retrograde chlorite replaces prograde biotite crystals by mimicking the foliation. Significant patches of late muscovite-sericite as well as chlorite overgrowing garnet are common textures in these rocks (Figure 5f). Sample 714-5F contains chlorite- and muscovite-filled veins that are consistently oriented parallel to each other throughout the sample and cross-cut the peak minerals (Figure S2d).

Some rocks with a darker-colored outcrop appearance within the metapelitic packages, commonly referred to as “mafic metapelites” (e.g., Nutman et al., 1984), have a more Ca- and Mg-rich composition than the typical metapelites (Rollinson, 2002). Two of such rocks (samples 714-5A and 729-1B) show peak assemblages of quartz + garnet<sub>syn</sub> + amphibole + plagioclase + ilmenite  $\pm$  calcite  $\pm$  sulfides  $\pm$  apatite. These are foliated rocks with garnet and amphibole (in the case of sample 729-1B) porphyroblasts that deflect the foliation. Garnets in sample 714-5A show inclusion-rich cores with curved patterns and inclusion-poor rims that overgrow the external foliation (Figure 4d), while garnets in sample 729-1B exhibit straight inclusions patterns or skeletal-like textures with smaller, more euhedral grains in the outer parts of the clusters (Figure S1i). Chlorite can be seen overprinting garnet and amphibole, as well as filling fractures in minerals as well as some fractures cross-cutting the rocks.

Sample 725-4A (described in the field as BIF) is a banded rock with four distinct mineralogical domains. One domain is very rich in amphibole that occurs as porphyroblasts with inclusions of quartz, biotite, and opaques. A second domain is dominated by quartz and magnetite, with minor occurrence of amphiboles following the foliation. In this band, a medium-grained epidote crystal ( $\approx 1,500 \mu\text{m}$ ) is surrounded by a corona of pink garnet and green amphibole, and the foliation is slightly deflected around the mineral (Figure 4g). A third, plagioclase-poor band is rich in quartz and biotite. This band is followed by another band with biotite, amphibole, garnet, and quartz. Garnet in this band occurs as porphyroblasts with curved inclusion patterns resembling in-places snow-ball fabrics (Figure 4h, Figure S1j).

The petrographic description of the different lithologies highlights the fact that retrogression is a common feature. Remarkably, mafic schist sample 729-5 collected in the northern part of the belt (Figure 1; zone B of Arai et al., 2015) represents an extreme example of low temperature greenschist facies overprint. This particular sample exhibits crenulation cleavage (Figure S1e) with inclusion-poor garnet porphyroblasts. The garnet crystals are replaced by randomly oriented biotite grains, which themselves are overprinted by chlorite (Figure 5g) that comprises most of the matrix along with few relic biotite grains (Figure 5h).

### 3.2. Mineral Chemistry

The chemistry data of the garnet, amphibole, biotite, and plagioclase can be found in Ramírez-Salazar et al. (2020a), some classification diagrams are shown in Figure S3 and the methodology is described in the Supportive information Text S1 and S3. For garnet from the metapelite sample 714-5E (Figure 6), we present a detailed mineral chemistry map (processed using XMapTools version 3.3.1; Lanari et al., 2014) exhibiting the commonly observed three zones. Notably, while the core (Grt<sub>1</sub>) and annulus (Grt<sub>2</sub>) zones exhibit a sharp change in chemistry, the inclusions trail is continuous from the core to the annulus (Figure 6a). Specifically, the garnet core (Grt<sub>1</sub>) shows low content in grossular ( $X_{\sim 3}^{\text{Gro}}$ ), rises steeply in the garnet annulus (Grt<sub>1</sub>;  $X_{3-8}^{\text{Gro}}$ ) and then falls to values similar to Grt<sub>1</sub> in the rim (Grt<sub>3</sub>; Figure 6b;  $X_{8-2}^{\text{Gro}}$ ). The almandine (Figure 6c) content shows a concave increase in Grt<sub>1</sub> ( $X_{75-85}^{\text{Alm}}$ ), followed by a nearly constant content in Grt<sub>2</sub> ( $X_{\sim 85}^{\text{Alm}}$ ) and a slight increment in Grt<sub>3</sub> ( $X_{85-89}^{\text{Alm}}$ ). The chemical map reveals no significant changes in pyrope content and a typical bell shape decrease in spessartine, with an almost constant content toward the rim (Figure 6d).

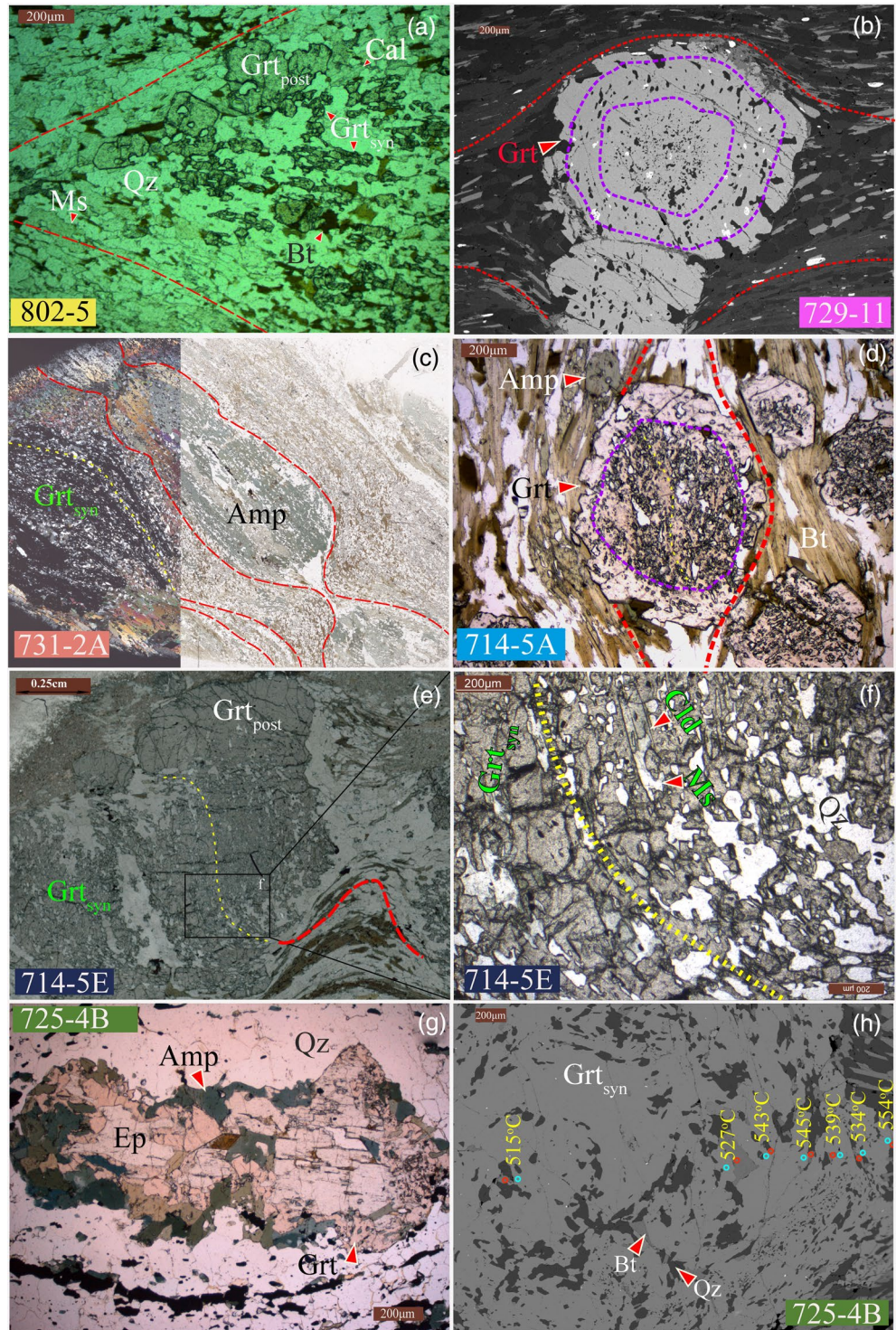


**Figure 4.** Photomicrographs showing peak mineralogy and microstructures. (a) Skeletal-like syn-tectonic garnets and euhedral post-tectonic grains; (b) garnet showing three different microstructural domains; (c) arc-like inclusions trails in garnet and boudinage structures; (d) garnet showing inclusion-rich core and inclusion-poor rims; (e and f) spiral-like garnet; (g) garnet-amphibole coronae on epidote; (h) Backscatter electron image of garnet showing garnet-biotite temperatures (Perchuk & Lavrent'eva, 1983) calculated along a grain transect. Scale in all images is the same (200  $\mu\text{m}$ ), except in (c and e). Red dotted lines indicate external foliation, yellow dotted lines internal garnet foliation, and purple dotted lines limit between garnet microstructural zones.

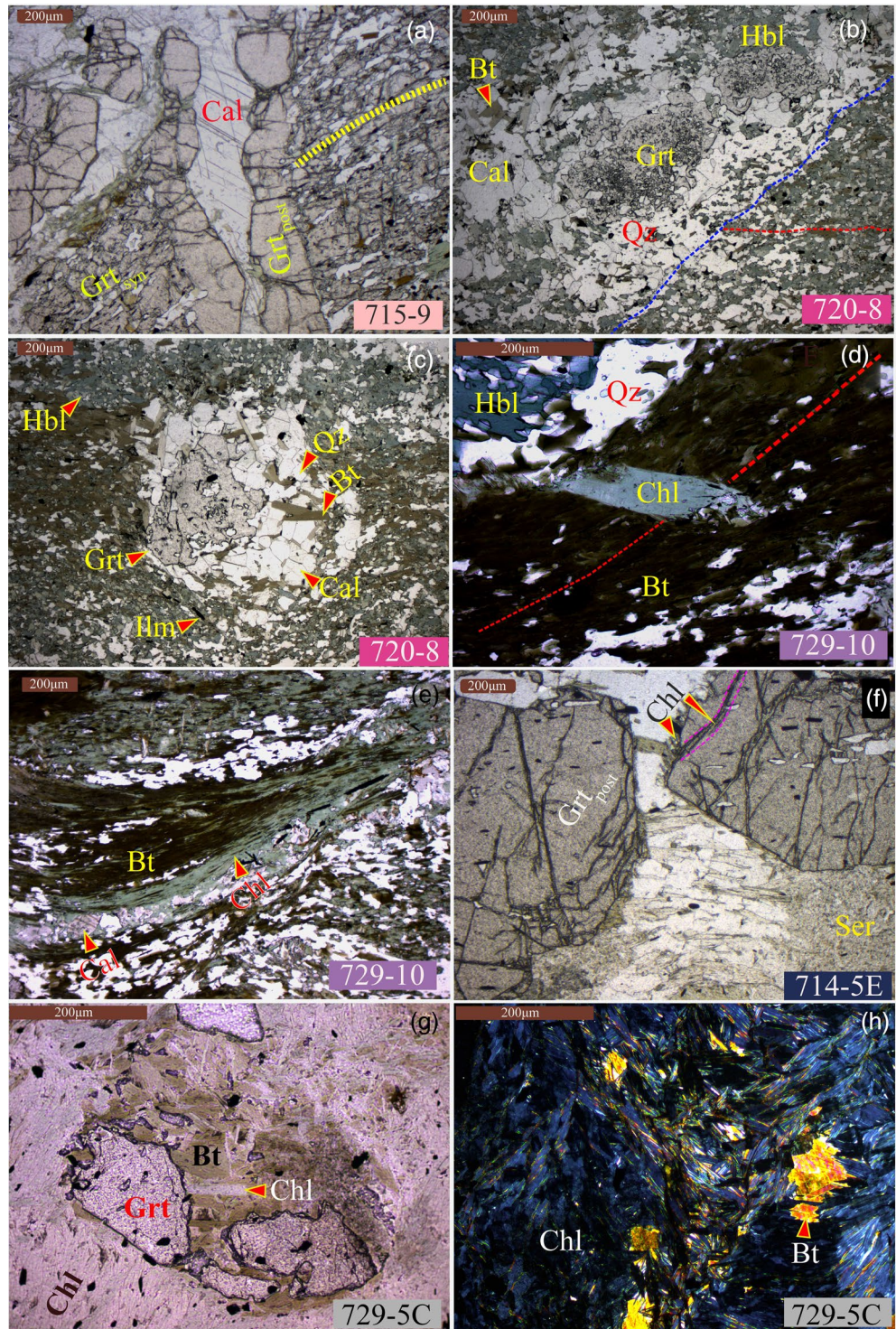


**Figure 5.** Post-tectonic medium- and low-temperature paragenesis and microstructures. (a) Calcite vein cross-cutting garnet internal foliation and post-tectonic euhedral garnet growing toward the vein center. (b) Late calcite veins cross-cutting the main foliation, which are overprinted by post-tectonic garnets. (c) Garnet replacement by calcite-quartz-biotite. Retrograde chlorite (d) overprints the foliation and (e) mimicks the foliation by replacing biotite and (f) growing along fractures that cross-cut post-tectonic garnet. (g) Biotite pseudomorphing garnet and chlorite replacing biotite. (h) Extreme biotite chloritization. Scale in all images is the same (200  $\mu\text{m}$ ). Red dotted lines indicate external foliation, yellow dotted lines internal garnet foliation and blue dotted lines limit of veins.

### 3.3. Thermobarometry

To determine the peak metamorphic conditions, we combined classic geothermobarometry utilizing mineral pairs or assemblages and thermodynamic isochemical phase modeling. We applied the garnet-biotite Fe-Mg exchange geothermometer (Perchuk & Lavrent'eva, 1983) on 11 samples and the Ti-in-Biotite geothermometer (Henry et al., 2005) on 13 samples across the ISB (Table 1). The calibration from Perchuk and Lavrent'eva (1983) was applied to be consistent and comparable with results from Rollinson (2002).

The temperature range (470°C–570°C) and mean values (490°C–530°C) derived from the exchange thermometer using garnet (cores) and biotite inclusions show no systematic increase in temperature from the northeast to the southwest (Figure 7a). The mean values of samples are very similar throughout the belt. For six of these samples (714-5A, 715-9, 717-5F, 715-16, 717-5, 725-4A, and 801-4), we obtained the chemical composition for inclusion-host mineral pairs along overall profile transects, which suggest an increase in temperature from core to rim that is typically not greater than 50°C (Figure 4h and Figure S4) in all the samples except 717-5F and 715-9, where the increment in temperature from core to rim is > 60°C, ranging from 505°C to 589°C and 468°C–535°C, respectively. Modeled temperatures using inclusion-poor rim analyses of garnet and adjacent matrix biotite generally returned temperatures <550°C, which are typically lower than those recorded in the cores (Figure 7b), with the exception of sample 725-2c that returned mean temperatures of 487°C in the core and 544°C in the rims (Figure 7b).

Temperatures obtained with the Ti-in-Bt geothermometer (Henry et al., 2005) range from 510°C to 650°C (Figure 7a and Figure S5) with the highest values returned from samples that are poor in ilmenite (e.g., 717-5) or with a low number of analysis (e.g., 729-1B, 720-8 and 730-2A;  $n < 4$ ). Apart from the samples showing temperatures in excess of 610°C, the mean temperature modeled for the rest of the biotite analyses in different ilmenite-rich rocks ranges from 540°C to 590°C (Figure 7a). Again, modeled temperatures yield no clear spatial pattern of systematic increase in temperatures in any direction such as North versus South, East versus West of ISB (Figure 7a, Figure S5). The values were obtained mainly in biotite crystals that are part of the peak assemblage and that make up the main foliation of the rocks (e.g., Figure 4d and Figures S1a, S1d, S1f) and some as inclusions in garnets (e.g., Figure 4h), with no clear temperature difference among these groups.

A total of eight isochemical phase diagrams have been calculated using the Perple-X software (Connolly, 2005; ver. 6.8.6) and the internally consistent database of Holland and Powell (2011, sd622). The calculations were performed in the MnNCKFMASHTO system for the metafelsic volcanics and metapelitic rocks and in the NCKFMASHTO system for the amphibolites. More detailed specifications regarding the use of activity models and input parameters, as well as methodology for the bulk-rock composition are listed in Text S2 and the compositions are reported in Ramírez-Salazar et al. (2020b) and shown in Tables S1 and S2. Results reveal that the overlap of stability fields covering the observed mineral assemblages do not show any systematic increase in pressure and/or temperature as a function of their spatial distribution (Figures 8 and 9 and Figure S6). Most of the samples converge in a range of 0.5–0.7 GPa and 550°C–600°C (Figure 9a). However, the stability fields of the two southernmost samples (725-2c and 725-3a) display higher temperatures from 585°C to 625°C and up to 700°C for 725-3a, with similar pressure values as the other samples (Figures 8e and 8f). To further constrain the stability conditions of the individual mineral assemblages, we plotted chemical isopleths for garnet compositions and other minerals from samples 714-5E (Figure 9c) 17725-2c (Figure 8d) 17725-3A (Figure 8f), as well as the modal isopleths for sample 17714-5A (Figure 8b). Here, we assume that the whole-rock composition of the samples and the selected a-x models are suitable for modeling the composition and abundances of the mineral in the rocks as isopleths; in that case, isopleths plot within or very close to the stability peak assemblage, possibly further limiting the stability of the rock within larger fields (e.g., Figures 8b, 8e, 8f and 9c). We also assume that the parameters used are suitable for modeling the evolution of the garnet cores, meaning that the intersection of the garnet end-member isopleths will define small P-T fields under which garnet grew, which could be different from those for the peak metamorphic assemblage (Figure 9c).

For sample 714-5A, the peak assemblage stability field indicates pressures of 0.36–0.68 GPa and temperatures of 540°C–610°C (Figure 8b), essentially reflecting the same temperature range obtained by garnet-biotite and Ti-in-Biotite geothermometry for the same sample (Figures 7a and 8b). The modal isopleths for

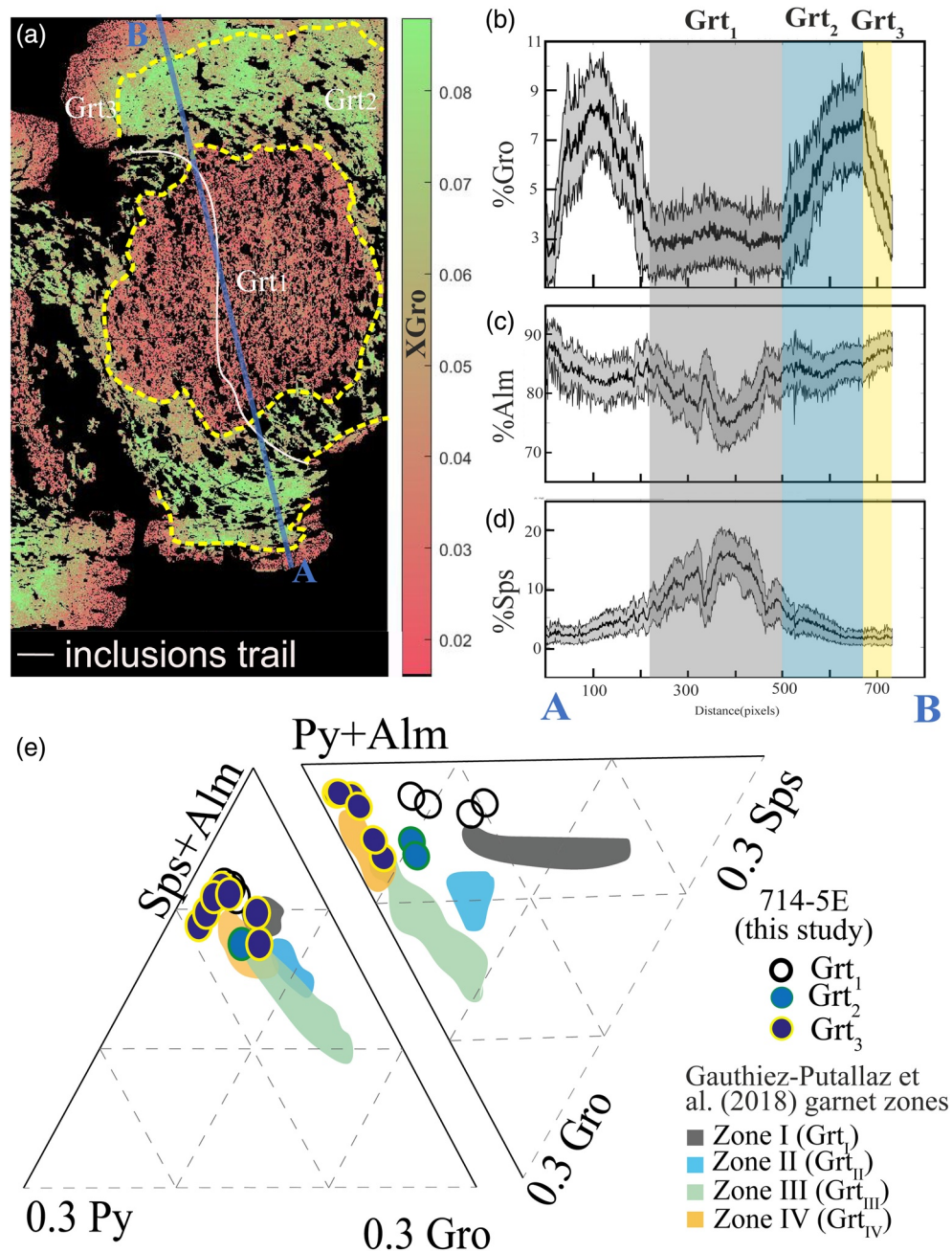


**Figure 6.** Geochemical characterization of spiral-like garnet in sample 714-5E. (a) Grossular content calibrated map and (b–d) compositional transects generated with XMapTools (Lanari et al., 2014). (c) Comparison of the different garnet zones composition presented in this work with Gauthiez-Putallaz et al. (2020) data.

garnet, plagioclase, and amphibole plot within the stability field of the peak assemblage (dotted lines in Figure 8b), showing that the a-x models used reproduce well the abundance of the minerals in the rock. Apart from pyrope, the rest of the end-members intersect in relatively small areas within the peak stability field (not shown).

Metapelite sample 714-5E is part of the same outcrop as sample 714-5A with no visible tectonic break between the two units. The equilibrium fields of these two samples and sample 714-5F, which also forms part of the same outcrop, overlap at 0.55–0.68 GPa and 550°C–590°C (Figure 9c), suggesting this is the range of peak conditions. We used the mean composition of the garnet core (Grt<sub>1</sub>) and garnet annulus (Grt<sub>2</sub>) to plot

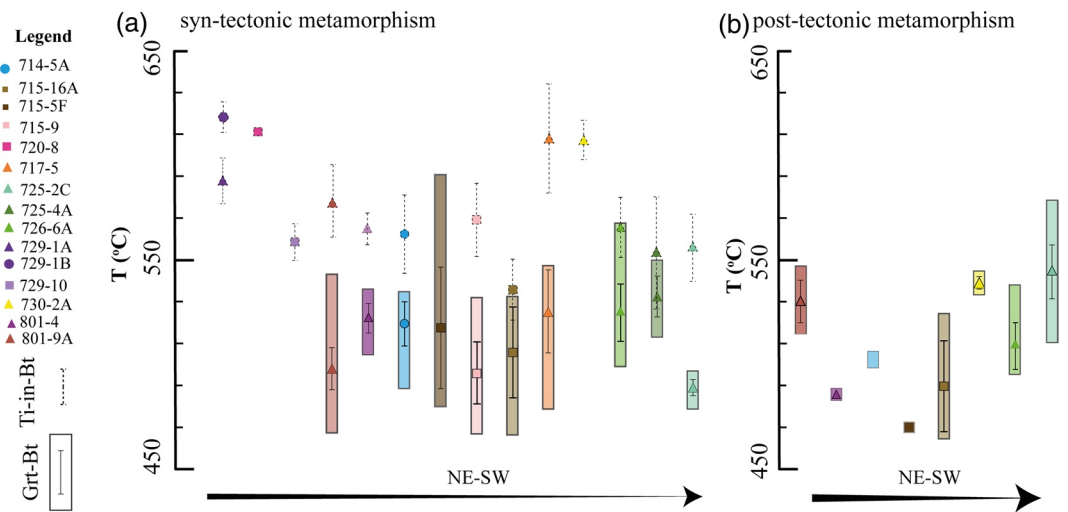


**Figure 7.** Classical geothermobarometry plots showing the mean (symbols with error bars) and range of (boxes) (a) temperature values for garnet-biotite calculations (Perchuk & Lavrent'eva, 1983) and (b) mean values returned from the Ti-in-Bt geothermometer (Henry et al., 2005).

the end-members isopleths of the solid solution (Figure 9c). Garnet compositional profile shows an increase in grossular content from core to annulus and decrease in spessartine content (Figure 6). In the plot illustrating the compositional intersection between Grt<sub>1</sub> and Grt<sub>2</sub>, the four garnet end-members isopleths define two narrow fields at 550°C, with the intersection for Grt<sub>2</sub> suggesting slightly higher pressures (Figure 9c). Both compositions plot at lower pressures than the field equilibrium assemblage of the rock, within a stability field with mineral assemblage showing Chl + Grt + St + Bt + Pl + Ilm + Qz. We note that the garnet core does show abundant inclusions of quartz and minor inclusions of ilmenite, chlorite, and plagioclase. However, the garnet core does not show any evidence of staurolite and, in contrast, contains chloritoid and muscovite (Figure 4f). These findings suggest that the onset of garnet growth forming the core started at lower pressure conditions ( $\approx 0.4$  GPa) followed by a nearly isothermal increase to form the mineral peak equilibrium assemblage ( $\approx 0.65$  GPa; Figure 9c).

An isochemical phase diagram calculated for sample 725-2c (Figure 8e), collected near the contact to the 3.7 Ga TTG in the southernmost part of the belt, shows a stability peak assemblage ranging from 600°C to  $>700^\circ\text{C}$  with similar pressures (0.4–0.7 GPa) as the samples collected further to the north (Figure 9a). We calculated the isopleths for the garnet end-members of the garnet core which define a narrow region  $\sim 580^\circ\text{C}$  and 0.5–0.7 GPa, plotting next to the stability field of the peak assemblage (green, yellow, and purple bands in Figure 8e). In contrast, the  $X_{\text{Mg}}$  biotite isopleths (pink band in Figure 8e) overlap within the peak stability field of 600°C–630°C, suggesting that this range as the maximum temperature the sample achieved.

Garnet-amphibolite sample 725-3a, collected just north of metafelsic volcanic sample 725-2c (Figure 1), apparently shows the highest metamorphic conditions in all the samples. The stability field of the peak assemblage expands from 550°C to 700°C, showing similar pressures as the other samples from 0.45 to 0.68 GPa. The isopleths for anorthite content in plagioclase, Ca content in amphibole (blue and cream bands respectively in Figure 8f), and garnet end-members intersect (green, red, and yellow bands in Figure 8f) within the stability field of the peak assemblage at temperatures  $>600^\circ\text{C}$  (Figure 8f).

## 4. Discussion

### 4.1. General Tectonometamorphic Evolution of the ISB—A Reappraisal

The detailed petrographic descriptions and metamorphic analyses presented in this work emphasize the complex textural-chemical relationships displayed in the rock record of the ISB, which essentially is the product of a poly-metamorphic history. Reading the rock record of such a geological setting is challenging

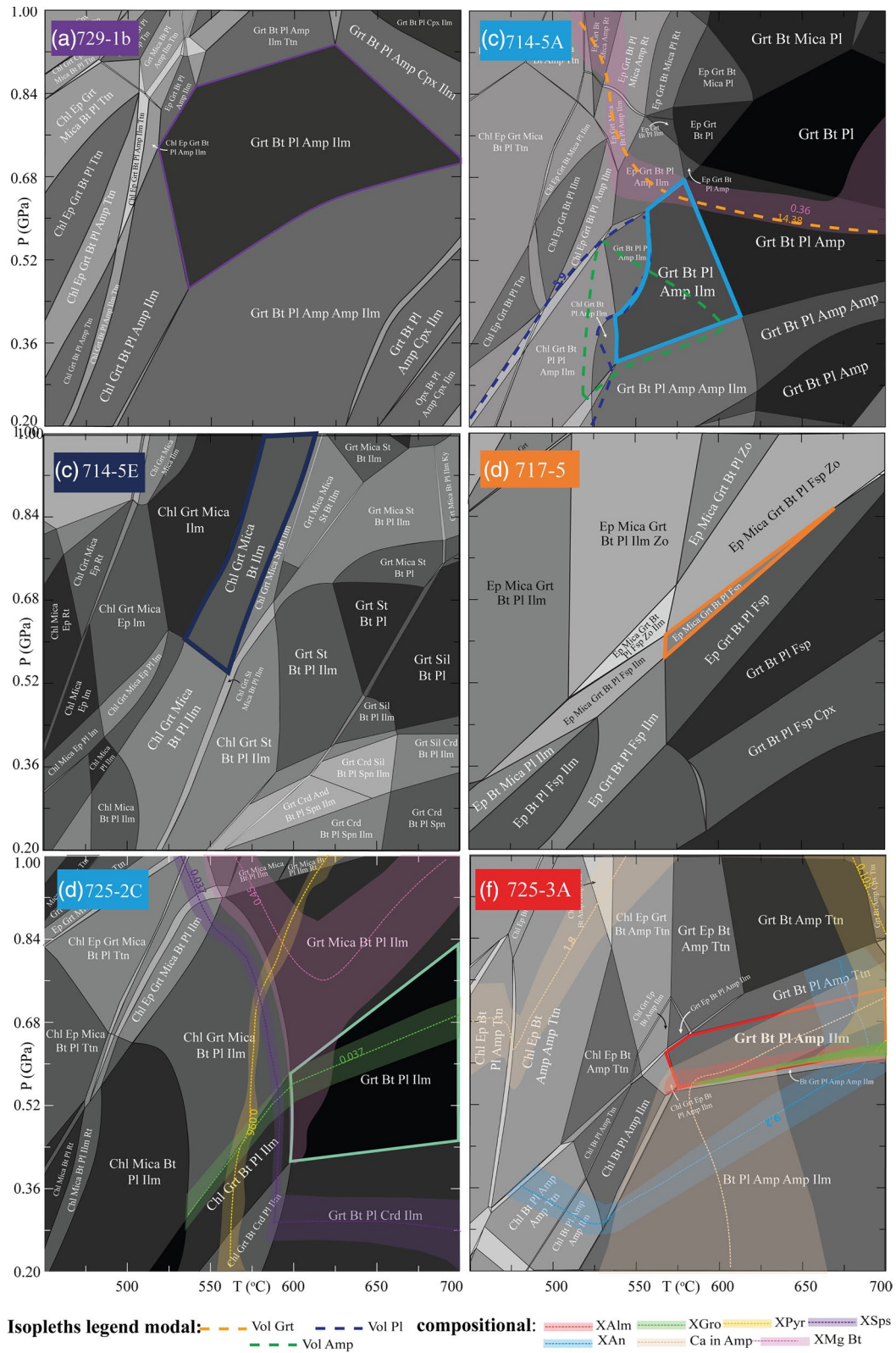


**Figure 8.** Isochemical phase diagrams calculated using Perple\_X (Connolly, 2005) in the MnNCKFMASHTO system with exception of samples 725-3a and 731-2A, calculated in the NCKFMASHTO system. All the phase diagrams were calculated assuming a water saturated system and  $Fe_2O_3 = 5\%$  (see Table S2). All fields contain quartz. Mineral abbreviations are after Whitney and Evans (2010). From (a-f) samples are arranged from northernmost to southernmost.

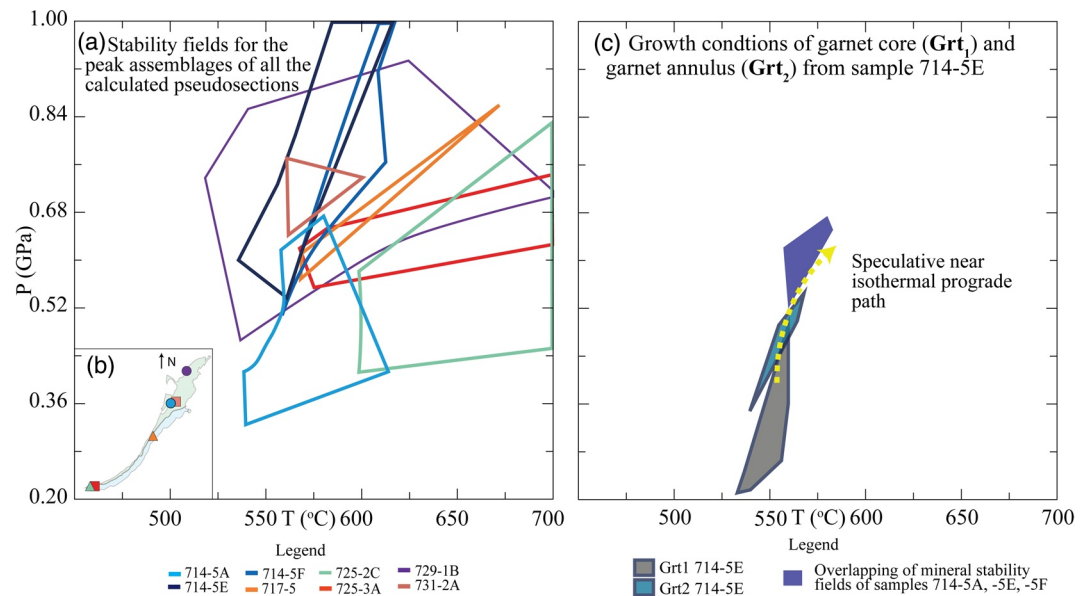


**Figure 9.** (a) Overlap of all the stability fields of the calculated isochemical phase diagrams and (b) their schematic positions in the eastern arm of the ISB; samples 714-5A, 714-5E, and 714-5F are from the same locality. (c) Stability fields created by the intersection of the garnet end-members for the core and annulus of garnet in samples 714-5-5E, suggesting a tentative isothermal path. ISB, Isua supracrustal belt.

and likely responsible for the existing contradictions in previous studies as outlined above. Based on our observations, we propose the occurrence of two medium temperature metamorphic events, followed by a pervasive low-temperature retrogression in the presence of variable amounts of fluid irrespective of terrane association and N-S location, whose characteristics we summarize below and illustrate in Figure 10. Even though we only present data from the well exposed eastern arm of the belt and mainly from the northeastern part, we assume our interpretations to be valid for the entire ISB.

The first event ( $M_1$ ) is recorded in most of the ISB rocks and is characterized by a distinct foliation and SE-plunging lineation with amphibolite facies mineral assemblages (Table 1) and common appearance of garnet and amphibole porphyroblasts (Figure 10a). Along the ISB from northeast to southwest, most samples display syn-tectonic inclusion-rich garnet cores, sometimes represented by curved (Figure 4c) or spiral-like (Figure 4e) inclusion trails that continue to the external foliation or sigmoidal garnets (see also Zuo et al., 2021). The common appearance of post-tectonic, inclusion-poor euhedral overgrowth rims marks the late, apparently static, medium-temperature metamorphic event ( $M_2$ ; Figure 10b), which has been reported to be ubiquitous everywhere in the belt (Rollinson, 2002, 2003). Some microstructures, like the calcite vein where euhedral garnet grows away from the walls (Figure 5a), suggest that this second generation of garnet growth might have been mediated by fluids in some parts of the belt.

As documented here and in existing studies (Rollinson, 2002, 2003), garnets in the Isua samples show a remarkable range of microstructures (Figure 4 and Figure S1), as well as chemical zoning patterns (Figure 6). Rollinson (2002) and other studies have linked them to up to three different medium-temperature metamorphic events: two in the early Archean and one in the late Archean (Gauthiez-Putallaz, 2020; Rollinson, 2002, 2003). Gauthiez-Putallaz et al. (2020) reported four chemical zones using major (Figure 6e) and trace elements and  $\delta^{18}\text{O}$  that match microstructural zones. The authors interpret that the core of their garnets ( $\text{Grt}_I$ ) represent an early Archean event at 550°C and the garnet annuli ( $\text{Grt}_{II\&III}$ ) represent later Eoarchean metamorphism at 610°C and 0.60 GPa (Figure 2), whereas the inclusion-poor rim ( $\text{Grt}_{IV}$ ) recorded final post-tectonic event in the late Archean (Figure 2). Garnets in sample 714-5E shows very similar major element zoning pattern, with three zones predominantly marked by the change in Ca composition (Figure 6). Our sample and sample G12/113 of Gauthiez-Putallaz et al. (2020) were collected within 50 m of each other and have similar bulk rock composition and mineralogy, and thus can

be assumed to have experienced the same tectonic history. When the compositions of the different zones within the garnets are compared, it is clear that they follow a similar pattern: the garnet cores form a separate compositional group in the ternary diagram of Py + Alm-Gro-Sps (Figure 6e), showing that they represent the same metamorphic event in both samples. The annuli and rim of both garnets also show similar trends (a relative Alm + Py enrichment toward the rim; Figure 6e) suggesting that the different zones recorded similar processes in both samples. However, we argue that the inner zones core-annuli (Grt<sub>1-2</sub> this study and Grt<sub>1-III</sub>, Gauthiez-Putallaz et al., 2020) represent only one tectono-metamorphic event (M<sub>1</sub>) instead of two based on our chemical-microstructural analysis (Figure 10a). Note that the inclusion trail in the garnet shows a remarkable continuity from the core to the annuli (Figures 4e, 4f and 6a), suggesting that they grew during a continuous deformation event so that the outline of the crystal shape would likely have followed the end of the inclusion trails. The observed chemical zonation pattern is not necessarily the product of different metamorphic episodes for garnet core, annuli, and the inclusion-poor rims, instead the observed chemical changes could be explained by the prograde path of the rock (see below) or by prolonged solid state diffusion. For example, an initial garnet with chemical growth zoning that is overgrown by an inclusion-free rim and experiencing diffusive re-equilibration is likely to produce a similar zoning pattern, where the original garnet grain boundary is obscured by diffusional re-equilibration. Examples of distorted zoning patterns following episodic overgrowth and diffusive relaxation are well documented for magmatic settings (e.g., Kahl et al., 2015) and are very likely to occur at prolonged amphibolite facies conditions (Müller et al., 2013). We note, however, that more work regarding specific diffusion models would be necessary to confirm this interpretation. In summary, we interpret the observed microstructures and chemical zoning to only represent two distinct medium-high temperature events (M<sub>1</sub> and M<sub>2</sub> in Figure 10) that might have experienced some diffusive re-equilibration rather than three distinct events.

Notably, Arai et al. (2015) suggests that retrogression in the ISB is negligible, whereas our results clearly demonstrate that, late low temperature retrogression forming mainly chlorite, muscovite, sericitization, and calcite (Figure 4) are commonly observed features across the belt, thus defining a distinct retrograde metamorphism (M<sub>3</sub>; Figure 10c) for the ISB, which is tightly linked to local presence of external fluid infiltration, suggested by the presence of calcite (Figures 5a and 5b) and chlorite veins (Figure 5f). Chlorite is one of the most abundant retrograde minerals in the studied samples: it occurs as individual grains or in veins cross-cutting and/or overgrowing the M<sub>1</sub> and M<sub>2</sub> assemblages (Figures 5c, 5f, and 5g). Interestingly, chlorite also mimics the foliation replacing biotite in various samples (e.g., Figure 5e). Retrogression and this type of chloritization are especially pronounced in the northeastern part of the ISB with an extreme example in sample 729-5, where biotite is pseudomorphing post-tectonic garnets revealing low-medium temperature retrogression (M<sub>3a</sub>; Figure 5g), followed by a nearly complete chloritization (M<sub>3b</sub>) of the rock (Figure 5h). These data are good examples of how retrogression can obliterate the peak assemblages while preserving the original fabrics (Figure 10c). We note that the distinction between potentially prograde chlorite and retrograde chlorite mimicking the foliation in the belt might be difficult to differentiate without more detailed observations, thus leading to the erroneous conclusion of an existing metamorphic gradient from the north, where retrogression is more pronounced, toward the south, which dominantly records the peak conditions most likely due to limited or even absence of external fluid infiltration. Thus, we argue that the greenschist assemblages, previously reported as prograde in the northern part of the belt, are essentially the product of poor preservation through enhanced metasomatism/retrogression (Figure 10c), and that the proposed medium P/T gradient (Arai et al., 2015) is likely a record of greenschist facies alteration rather than a record of southward-increasing peak metamorphic conditions. This interpretation is also supported by field observations that document enhanced alteration and metasomatism reflected in an increase in quartz-calcite vein density (Webb et al., 2020).

#### 4.2. Quantitative P-T Constraints

Both quantitative and qualitative P-T data have been published for the ISB and related rocks by various groups (Arai et al., 2015; Boak & Dymek, 1982; Dymek et al., 1988; Nutman et al., 2013, 2020). However, a discussion about the nature and extent of the observed differences in these estimations is still elusive. In this section, we discuss our P-T results in the light of previously published data.

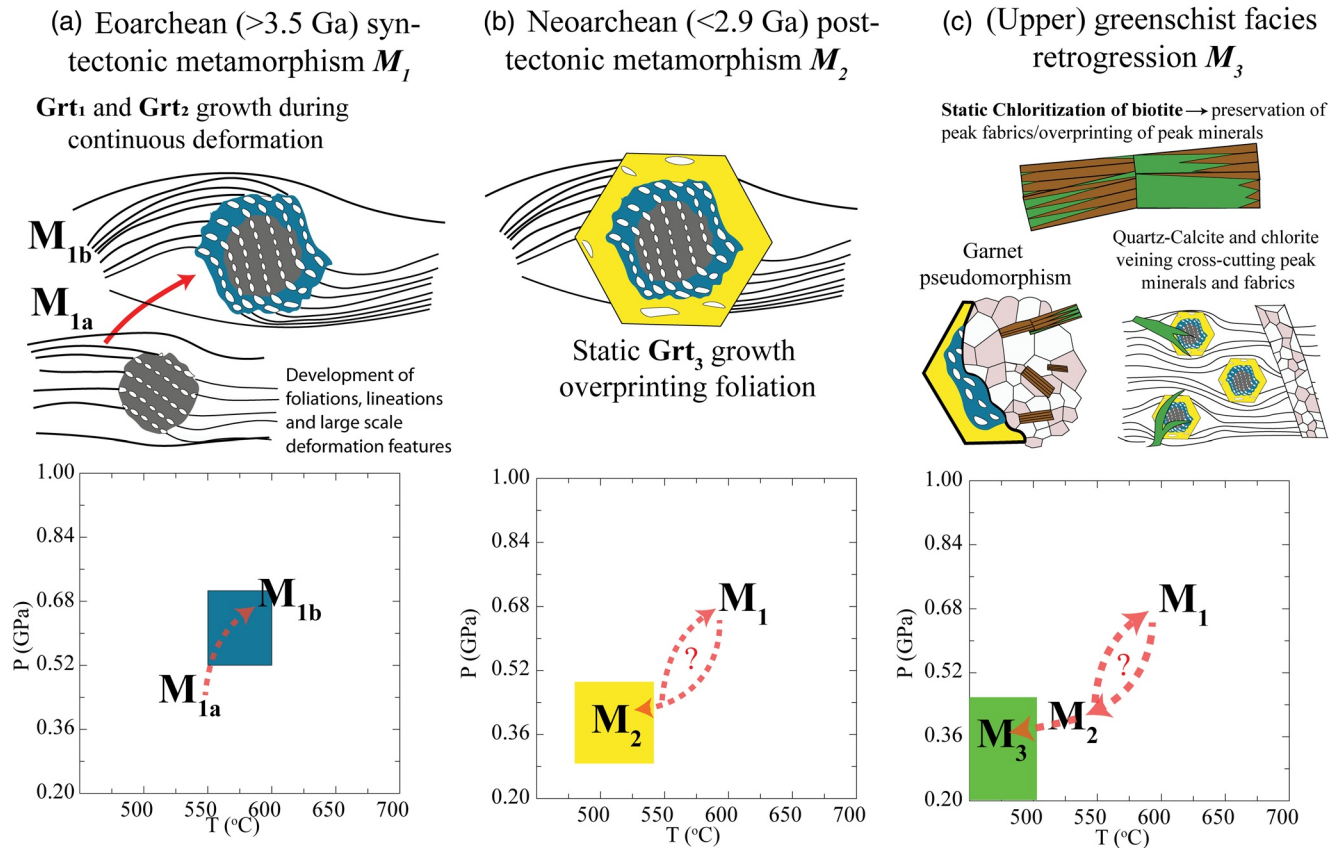


**Figure 10.** Metamorphic evolution of the ISB. Schematic representation of the microstructures and chemical zoning developed as well as range of pressure and temperature estimated for (a) the Archean syn-tectonic metamorphism, (b) Neoproterozoic post-tectonic metamorphism and (c) low-temperature static retrogression. P-T diagrams show tentative P-T paths. Samples studied show signatures of these three different events irrespective of their location within the belt. ISB, Isua supracrustal belt.

Classic geothermometry (Figure 7) and phase equilibria modeling (Figures 8 and 9) demonstrate a consistency of P-T values recorded by the rocks across most of the ISB. From north to south, the samples reveal similar temperatures when applying the garnet-biotite geothermometer (Figure 7), and our results fall within the same range as previous garnet-biotite calculations for the Eoarchean (Figure 1, 510°C–650°C; Boak & Dymek, 1982; Rollinson, 2002). Nevertheless, the results tend to return lower values than those reported by Rollinson (2002), although both studies applied the same calibration of Perchuk & Lavrent'eva (1983). This could potentially be the consequence of increased late stage alteration being more pervasive in our samples. To complement our thermometry data set, we also applied the Ti-in-Bt geothermometer (Henry et al., 2005) to our samples. However, these results (Figure 7, Figure S6) should be considered with caution as the geothermometer was empirically calibrated in ilmenite/rutile-bearing metapelites, and most of our samples cannot be classified as this type of lithology, although most samples do show titanium saturation (e.g., significant presence of ilmenite; Table 1). For comparison, we also applied the thermometer to five ilmenite-bearing metapelites reported by Boak and Dymek (1982), obtaining temperatures ranging from 558°C to 580°C (Figure 1). The mean temperature for most of our samples fall within this range, indicating that our Ti-in-Bt results (Figure 7) are generally a good proxy for the peak conditions of the ISB confirming a homogeneous distribution of metamorphic conditions throughout the belt.

Thermodynamic modeling of our samples reveals that most of the modeled stable assemblages overlap at 0.5–0.7 GPa and 550°C–600°C (Figure 9a), which we interpret as the best estimation for the peak syn-tectonic metamorphism of the entire ISB ( $M_1$ ; Figure 10a). These conditions are consistent with the Ti-in-Bt and the highest garnet-biotite values (Figure 7), as well as previous estimations (Boak & Dymek, 1982;

Rollinson, 2002). However, two samples collected from the southernmost part of the belt (725-2c and 3a) show higher temperature conditions ( $>600^{\circ}\text{C}$ ; Figures 8e and 8f). On the one hand, isopleth thermometry in the metafelsic volcanic sample 725-2c suggests that the garnet core equilibrated at  $570^{\circ}\text{C}$ – $600^{\circ}\text{C}$  at pressure  $>0.5$  GPa and that the possible maximum temperature of equilibrium is  $625^{\circ}\text{C}$ , according to biotite isopleth and the peak equilibrium assemblage (Figure 8e). On the other hand, the thermodynamic modeling of the garnet-amphibolite sample 725-3a, collected from adjacent to the 3.7 Ga tonalite and less than 0.5 km to the east of sample 725-2c, shows a peak assemblage equilibrium field that expands from  $550^{\circ}\text{C}$  to  $700^{\circ}\text{C}$  at similar pressures to the rest of the samples (0.5–0.7 GPa; Figure 8f). Moreover, most of the element isopleths for different minerals in the sample (e.g., amphibole, plagioclase, and garnet; colored bands in Figure 8f) intersect this stability field at  $T > 625^{\circ}\text{C}$ , suggesting significantly higher temperatures than those recorded in the rest of the samples. Notably, the outcrops of samples 725-2c and 725-3a are located relatively close to each other (Figure 1), and we take a conservative approach to assume both of the samples experienced similar peak metamorphic conditions ranging from  $570^{\circ}\text{C}$  to  $625^{\circ}\text{C}$  at 0.5–0.7 GPa, falling in the same PT range as the rest of the rocks. This is consistent with the quartz fabric thermometer applied to sample 725-2c, calculating deformation temperatures ranging from  $500^{\circ}\text{C}$  to  $650^{\circ}\text{C}$  (Zuo et al., 2021). The fact that the pressure estimations are consistent throughout the belt from north to south suggests that the rocks were subjected to similar burial conditions during the syn-tectonic metamorphism and that the apparent slightly higher temperatures recorded only in the southernmost samples are most likely to be a consequence of uncertainties in the thermodynamic models or potentially local slightly anomalous higher heat influx rather than reflecting a distinctly different tectonic environment. In general, the syn-tectonic metamorphic record ( $M_1$ ) of the Isua supracrustal rocks reveals a dominance in amphibolite facies metamorphism with no clear spatial metamorphic gradient (Figures 9a and 9b).

The combination of the compositional garnet profiles and the thermodynamic modeling potentially provides insights into the prograde evolution of  $M_1$ . As discussed in previous sections, the sharp compositional changes in the garnets clearly record the same deformation event as shown by the microstructures preserved in sample 714-5E (Figures 4e, 4f, and 6a). The chemical zoning then could be a consequence of the metamorphic path experienced by the rock and/or late diffusion. Gauthiez-Putallaz et al. (2020) already suggested an increase in pressure from core to annuli based on the lack of Eu negative anomaly in the annuli, which is indicative of plagioclase being consumed, typically associated to the increase in pressure (e.g., Spear et al., 1990). We plotted the mean composition (intersection of compositional isopleths) of  $\text{Grt}_1$  (core) and  $\text{Grt}_2$  (annulus) for sample 714-5E. The narrow stability field for the garnet core plots at lower pressures than, but similar temperatures to the annulus, suggesting that the samples experienced a near isothermal prograde path from 0.40 to 0.65 GPa at  $\sim 580^{\circ}\text{C}$  (Figures 9c and 10b). Spear et al. (1990) stated that garnet growing in equilibrium along an isothermal prograde path in a classic metapelite would show compositional profiles with increasing grossular component and to a lesser extent, almandine content, accompanied by a decrease in the spessartine component and a near flat profile of pyrope. These predictions are remarkably similar to the observed compositional profile of the spiral-like garnet in the metapelite sample 714-5E (Figure 6). However, given the uncertainties on the thermodynamic activity models, the apparent differences in pressure determinations within garnet core and annulus might be the artificial product of chosen parameters for the modeling and further work is needed to test the validity of this interpretation.

The garnet euhedral rims–matrix biotite pairs provide thermal constraints for the conditions of garnet overgrowth ( $M_2$ ). The calculated temperatures here range from  $470^{\circ}\text{C}$  to  $580^{\circ}\text{C}$ , with most of the values  $<540^{\circ}\text{C}$  (Figure 7b), which might be the best estimate and in agreement with previous studies that report similar results (Figure 1; Boak & Dymek, 1982; Gauthiez-Putallaz et al., 2020; Rollinson, 2002, 2003). Gauthiez-Putallaz et al. (2020) report post-tectonic garnet rims in the metapelites to show negative Eu anomaly, suggesting plagioclase crystallization during  $M_2$ . According to our thermodynamic modeling, plagioclase in the metapelites at  $T < 540^{\circ}\text{C}$  appears at pressures  $<0.5$  GPa (Figure 8c and Figure S6a) putting a maximum limit to the pressure conditions of  $M_2$  (Figure 10b). For  $M_3$ , we did not obtain any quantitative data for the P-T conditions, however, the prevalence presence of (upper) greenschist facies minerals such as chlorite, sericite and calcite suggest temperatures  $<500^{\circ}\text{C}$  (Figure 10c) for the retrograde metamorphism.

#### 4.2.1. Comparison With Previous Interpretations of the Metamorphic Record of the ISB

Our results for the peak metamorphic conditions of  $M_1$  contrast the interpretation of Arai et al. (2015) who suggest that the northeastern part of the belt could be divided into four different zones (A-D, Figure 1), with zone A and B showing upper greenschist facies assemblages ( $<500^\circ\text{C}$  and  $<0.6$  GPa). While we did not quantitatively study samples from zone A, our qualitative petrographic results and field data (Webb et al., 2020) clearly demonstrate that some samples experienced very pervasive retrogression in zone B (e.g., 729-5, Figures 5g and 5h) and that retrograde greenschist facies minerals such as chlorite can mimic the foliation (Figure 5e). Therefore, calculated greenschist conditions could actually represent the retrograde metamorphism ( $M_3$ ; Figure 10c) for zone B, which we assume is also true for zone A. Here, our modeled isochemical phase diagram from sample 729-1B, the proxy temperatures from Ti-in-Bt in sample 729-1A and 729-1B, in addition to quartz fabric thermometry presented in the corresponding part of this study (Zuo et al., 2021), all agree with  $T > 550^\circ\text{C}$  for samples located in zone B and thus showing similar conditions to those reported for zones C and D by Arai et al. (2015). However, Arai et al. (2015) also reported P-T estimations for three samples in zone C and three in zone D (Figure 1) using isochemical phase diagrams, and concluded that there is an increase in both pressure and temperature from zone C (0.4–0.7 GPa,  $500^\circ\text{C}$ – $600^\circ\text{C}$ ) to zone D (0.5–1.1 GPa,  $540^\circ\text{C}$ – $800^\circ\text{C}$ ). Careful inspection of the diagrams, however, reveals that only a single calculated stability field of a reported mineral assemblages (sample K755, located in the 3.8 Ga belt) extends to pressures and temperatures higher than 0.8 GPa and  $650^\circ\text{C}$ . All mineral assemblages reported for zone C and D overlap around  $550^\circ\text{C}$ – $600^\circ\text{C}$  and 0.5–0.7 GPa (Figure 12 in Arai et al., 2015), which is indistinguishable from the range of conditions presented in this work. As such, the results of Arai et al. (2015) show no clear systematic increase in metamorphic conditions, and hence there is no clear evidence of a metamorphic gradient from north to south, in consonance with our results.

The data presented here and the spatial resolution given by our samples do not a priori rule out an increase in pressure and temperature toward the center of the 3.70 Ga TTG body (Nutman et al., 2013) nor the record of paired metamorphism interpreted from the TTGs/zircon chemistry and granulites (Nutman et al., 2020). However, our results convincingly demonstrate that both the 3.7 and 3.8 Ga belts record similar peak conditions for  $M_1$ , arguing that at least for the supracrustal rocks there is no clear metamorphic gradient. Moreover, we propose that the chemical record of the TTGs/zircon and the mineralogy of the granulites of the IGC can be explained in simpler terms with the available data reported in the literature and that they do not necessarily record paired metamorphism. Using Isua tholeiitic basalts as starting composition and phase equilibria modeling, Hoffman et al. (2019) showed that melts in equilibrium with garnet and rutile formed at 1.3 GPa and  $885^\circ\text{C}$ – $1020^\circ\text{C}$ , and melts in equilibrium with orthopyroxene-granulites that formed at 0.8 GPa and  $870^\circ\text{C}$ – $980^\circ\text{C}$  would have a similar major and trace element chemistry as observed in the natural TTG samples of the Itsaq Gneiss Complex. In their model, the stability field of the orthopyroxene-granulites expands up to 1.1 GPa (Figure S7), suggesting that tonalites with no garnet signature can be produced in T/P gradients as low as  $800^\circ\text{C}/\text{GPa}$ , while those with residual garnet would have been generated at  $T/P \approx 700^\circ\text{C}/\text{GPa}$  (Figure S7). Therefore, (1) the presence or absence of a garnet signature in the tonalite/zircon chemistry does not necessarily represent two very different gradients ( $<500^\circ\text{C}$  vs.  $>1000^\circ\text{C}/\text{GPa}$ , respectively); and (2) the geochemical record of the plutonic bodies, as well as the appearance of a garnet granulite and an orthopyroxene granulite could be easily explained within a much narrower P-T field (Figure S7) with a gradient ranging from  $\approx 700^\circ\text{C}$  to  $\approx 900^\circ\text{C}/\text{GPa}$ . This range is in agreement with independent estimations (e.g., Gardiner et al., 2019) and fall within the gradient obtained from our peak mineral conditions. While our analyses benefit from geologically constrained data within Isua and the Itsaq Gneiss Complex, Nutman et al. (2020) uses a more generalized approach applying simplified mineral reactions in P-T space as well as a simplified estimate of the general parent material composition (MORB) that may or may not be appropriate to represent geochemical and mineralogical characteristics of the Archean record protolith (e.g., Johnson et al., 2017; Smithies et al., 2009). We therefore conclude that more detailed P-T data are needed for the samples reported by Nutman et al. (2020) to be able to retrieve and compare changes in their metamorphic record and, most importantly, assess the possible presence or absence of paired metamorphism.

#### 4.3. Implications for the Tectonic Evolution of the Isua Supracrustal Belt

The data and discussion presented in this work have profound implications evaluating the validity of the three different tectonic models that are currently put forward for the evolution of Isua (Figure 3). Two vari-

ants of horizontal tectonic models interpret the pervasive deformation and metamorphism throughout the ISB as a product of subduction and/or collision of the 3.7 and 3.8 Ga belts (Figures 3a and 3b; Arai et al., 2015; Komiya et al., 1999; Nutman & Friend 2009). Both predict, accordingly, the development of a systematic metamorphic gradient across the area (Arai et al., 2015; Nutman et al., 2013, 2020). However, petrography and extracted P-T constraints presented here are inconsistent with any north-south metamorphic gradient predicted by the south-dipping subduction model (Figure 3a; Arai et al., 2015; Hayashi et al., 2000; Komiya et al., 1999). The limited thickness of the belt and the distribution of our samples precludes the necessary spatial resolution of P-T data to adequately test the existence of an east-west gradient toward the interior of the 3.7 Ga TTG and with that the viability of the north-dipping subduction model (Figure 3b; Nutman et al., 2013). Notwithstanding, our results confirm amphibolite conditions for the 3.8 Ga part of the belt which contrast the reported greenschist facies peak conditions for this belt based on field observations (Nutman et al., 2013). The north-dipping model argues further that the garnet cores in the 3.7 Ga belt record a different tectono-metamorphic event (Gauthiez-Putallaz et al., 2020), related to the formation of a 3.7 Ga proto-arc in a subduction zone (Nutman et al., 2015). However, this study's garnet analyses results offer an alternative, more prudent interpretation of the different core-annuli garnet domains, suggesting that they do not necessarily reflect different tectonic events, but rather a continuous metamorphic-deformation episode. Furthermore, our evidence is consistent with homogenous metamorphism all along the belt rather than a systematic metamorphic gradient. In summary, our results and existing geochemical, isotopic, and structural data could be equally, if not better be explained by the predictions of nonuniformitarian models.

Vertical tectonic regimes such as the heat-pipe model (Moore & Webb, 2013) predict that the ISB was emplaced as a continuous volcano-sedimentary sequence formed by rapid resurfacing events and subsequent crustal melting to generate the TTGs (Webb et al., 2020). This model (Figure 3c) provides a scenario consistent with the data presented here as well as reported field relationships. The model predicts an amphibolite facies metamorphism across the entire ISB, that was syn-tectonic to deformation related to shearing that folded the volcano-sedimentary sequence (Figures 3c and 10a) which is inferred by the A-type fold geometry of the ISB (Webb et al., 2020). Additional support for the viability of a heat-pipe like model are the following observations: (1) the model allows for the formation of a stable crust necessary to generate the reported multiple melting events directly related to TTG emplacement (Hiess et al., 2011; Hoffmann et al., 2014); (2) nearly nonexistent contamination of the igneous rocks consistent with the efficient extrusion of hot materials envisaged (Polat et al., 2002); (3) rapid resurfacing and burial inhibit the sedimentary recycling of the older units and allows for continuous basalt-surface water interactions that is required to produce the oxygen isotopic composition of the TTG zircons from melting of a deep seated hydrated basaltic source (Hiess et al., 2009). Furthermore, A-type folding explains the two opposing shear senses and the quasihomogenous strain intensities recorded in the macro- and microstructures across the belt (Zuo et al., 2021). Thus, in summary, we argue that the syn-metamorphic record of the ISB is more easily explained with the predictions of heat-pipe model rather than a plate tectonic scenario which would predict significant spatial differences in recorded peak metamorphic grade both in temperature and pressure. However, as expected by the constraints of the heat-pipe model, a previous burial metamorphism must have affected the ISB. The microstructures and minerals of this earliest recorded event (Pre-M<sub>1</sub>, Figure 10a) were probably completely recrystallized and replaced during the pervasive syn-tectonic deformation, but some relics might have been preserved in the cores of some of the garnets exhibiting randomly oriented inclusions (Figure 4b and Figure S1f). Further studies on those cores could give inside on the changes in pressure from the 3.7 Ga to the 3.8 Ga belts, to test the model of a continuous thickened supracrustal sequence.

## 5. Conclusions

The ISB is one of the best preserved >3.5 Ga terranes and its study has been crucial to our understanding of Early Earth processes. However, the nature of its metamorphic record has long been overlooked, despite it being key to understanding the tectonic evolution of the belt. Our comprehensive study on the metamorphism of the ISB provides new microstructural and thermobarometric data that allows us to reconcile previously published interpretations and contradictions of the metamorphic history of the ISB. Our study shows that:

- Petrographic observations shed light on the problem of preservation of the metamorphic record. Our observations reveal significant overprinting of peak assemblage by retrograde minerals while preserving the original fabrics (e.g., the penetrative external foliation, Figures 5e and 10c). Such selected preservation may have led to previous misinterpretations of the metamorphic record
- The combination of microstructural analysis and chemical zoning applied to garnet offers a simpler explanation for the different compositional zones within garnet typical of the ISB, showing that the core and annuli grew during a continuous tectono-metamorphic event (Figure 10a), followed by a post-tectonic metamorphism recorded in garnet rims overgrowing the syn-tectonic fabrics (Figure 10b)
- The ISB experienced at least three distinct metamorphic events recognizable throughout the belt (Figure 10): a  $M_1$  event defined by nearly homogeneous syn-tectonic amphibolite facies metamorphism with peak conditions at 550°C–600°C and 0.5–0.7 GPa; a  $M_2$  lower amphibolite facies (<540°C and <0.5 GPa) post-tectonic thermal event; and a  $M_3$  event defined by (upper) greenschist facies (<500°C) pervasive retrograde metamorphism associated with local brittle failure and fluid infiltration
- The metamorphic and geological records of the ISB are consistent with nonuniformitarian, preplate tectonic models

Our findings on the poly-metamorphic history of the ISB do not necessarily exclude the possibility of horizontal movements during its evolution. However, the metamorphic evidence presented in this work and previously published data argue that the early Archean evolution of the ISB is consistent with a regime dominated by heat-pipe tectonics. Thus, the ISB provides direct evidence that the Early Archean geodynamics was distinct to that of modern Earth. We stress that, despite the evidence presented here, a more detailed and spatially constraint P-T-X-t-d evolution of the ISB, as well as petrochronological constraints on the different metamorphic events are necessary develop a time constraint tectonic model for Isua.

## Data Availability Statement

Data used in this work are available in the figures, tables, supporting information, and data sets submitted along this manuscript, the mineral chemistry and bulk rock data can be obtained from the EarthChem repository (<https://doi.org/10.26022/IEDA/111667> and <https://doi.org/10.26022/IEDA/111668>).

## Acknowledgments

Sample collection for this study was supported by a Seed Fund for Basic Research grant (project code: 201610159002) to AAGW and TM as well as start-up funds to AAGW, both from the University of Hong Kong. Some of the funds for the analytical work was supported by the Hong Kong Research Grants Council via a General Research Fund grant (project code: 17305718) to AAGW. We would like to thank Richard Walshaw and Jürgen Neubauer for their assistance in processing and acquisition of the microprobe data, Lesley Neve for the acquisition of the XRF data and training for XRF sample preparation, and John Wyn Williams for the training and assistance in the thin section preparation. We would like to thank Benita Putlitz and Lukas Baumgartner for the discussions that enriched an earlier version of this manuscript. Matthijs A. Smit and Hugh Rollinson are gratefully acknowledged for their constructive reviews that significantly improved this contribution. Anthony Ramirez-Salazar thanks the CONAcYT scholarship that supports his PhD studies.

## References

- Abbott, D., Drury, R., & Smith, W. H. F. (1994). Flat to steep transition in subduction style. *Geology*, 22(10), 937–940. [https://doi.org/10.1130/0091-7613\(1994\)022<0937:FTSTIS>2.3.CO;2](https://doi.org/10.1130/0091-7613(1994)022<0937:FTSTIS>2.3.CO;2)
- Allwood, A. C., Rosing, M. T., Flannery, D. T., Hurowitz, J. A., & Heirweh, C. M. (2018). Reassessing evidence of life in 3,700-million-year-old rocks of Greenland. *Nature*, 563(7730), 241–244. <https://doi.org/10.1038/s41586-018-0610-4>
- Appel, P. W. U., Rollinson, H. R., & Touret, J. L. R. (2001). Remnants of an early Archean (>3.75 Ga) sea-floor, hydrothermal system in the Isua Greenstone Belt. *Precambrian Research*, 112(1–2), 27–49. [https://doi.org/10.1016/S0301-9268\(01\)00169-3](https://doi.org/10.1016/S0301-9268(01)00169-3)
- Arai, T., Omori, S., Komiya, T., & Maruyama, S. (2015). Intermediate P/T-type regional metamorphism of the Isua supracrustal belt, southern west Greenland: The oldest Pacific-type orogenic belt? *Tectonophysics*, 662, 22–39. <https://doi.org/10.1016/j.tecto.2015.05.020>
- Blichert-Toft, J., & Frei, R. (2001). Complex Sm-Nd and Lu-Hf isotope systematics in metamorphic garnets from the Isua supracrustal belt, West Greenland. *Geochimica et Cosmochimica Acta*, 65(18), 3177–3189. [https://doi.org/10.1016/S0016-7037\(01\)00680-9](https://doi.org/10.1016/S0016-7037(01)00680-9)
- Boak, J. L., & Dymek, R. F. (1982). Metamorphism of the ca. 3800 Ma supracrustal rocks at Isua, West Greenland: Implications for early Archean crustal evolution. *Earth and Planetary Science Letters*, 59(1), 155–176. [https://doi.org/10.1016/0012-821X\(82\)90123-6](https://doi.org/10.1016/0012-821X(82)90123-6)
- Bridgwater, D., Watson, J., & Windley, B. F. (1973). The Archean craton of the North Atlantic region. *Philosophical Transactions of the Royal Society A: Mathematical, Physical & Engineering Sciences*, 512, 493–512.
- Brown, M. (1993). P-T-t evolution of orogenic belts and the causes of regional metamorphism. *Journal of the Geological Society*, 150, 227–241.
- Brown, M. (2010). Paired metamorphic belts revisited. *Gondwana Research*, 18(1), 46–59. <https://doi.org/10.1016/j.jgr.2009.11.004>
- Brown, M., & Johnson, T. (2018). Secular change in metamorphism and the onset of global plate tectonics. *American Mineralogist*, 103(2), 181–196. <https://doi.org/10.2138/am-2018-6166>
- Collins, W. J. (1989). Polydiapirism of the Archean Mount Edgar Batholith, Pilbara Block, Western Australia. *Precambrian Research*, 43(1–2), 41–62. [https://doi.org/10.1016/0301-9268\(89\)90004-1](https://doi.org/10.1016/0301-9268(89)90004-1)
- Connolly, J. A. D. (2005). Computation of phase equilibria by linear programming: A tool for geodynamic modeling and its application to subduction zone decarbonation. *Earth and Planetary Science Letters*, 236(1–2), 524–541. <https://doi.org/10.1016/j.epsl.2005.04.033>
- Crowley, J. L. (2003). U-Pb geochronology of 3810–3630 Ma granitoid rocks south of the Isua greenstone belt, southern West Greenland. *Precambrian Research*, 126(3–4), 235–257. [https://doi.org/10.1016/S0301-9268\(03\)00097-4](https://doi.org/10.1016/S0301-9268(03)00097-4)
- Crowley, J. L., Myers, J. S., & Dunning, G. R. (2002). Timing and nature of multiple 3700–3600 Ma tectonic events in intrusive rocks North of the Isua greenstone belt, southern West Greenland. *Bulletin of the Geological Society of America*, 114(10), 1311–1325. [https://doi.org/10.1130/0016-7606\(2002\)114<1311:TANOMM>2.0.CO;2](https://doi.org/10.1130/0016-7606(2002)114<1311:TANOMM>2.0.CO;2)

- Dhuime, B., Hawkesworth, C. J., Cawood, P. A., & Storey, C. D. (2012). A change in the geodynamics of continental growth 3 billion years ago. *Science*, 335(6074), 1334–1336. <https://doi.org/10.1126/science.1216066>
- Dymek, R. F., Brothers, S. C., & Craig, M. (1988). Petrogenesis of ultramafic metamorphic rocks from. *Journal of Petrology*, 29, 1353–1397.
- Ehlers, K., & Hoinkes, G. (1987). Titanian chondrodite and clinohumite in marbles from the Ötztal crystalline basement. *Mineralogy and Petrology*, 36(1), 13–25. <https://doi.org/10.1007/BF01164366>
- Frei, R., Bridgwater, D., Rosing, M., & Stecher, O. (1999). Controversial Pb-Pb and Sm-Nd isotope results in the early Archean Isua (West Greenland) oxide iron formation: Preservation of primary signatures versus secondary disturbances. *Geochimica et Cosmochimica Acta*, 63(3–4), 473–488. [https://doi.org/10.1016/S0016-7037\(98\)00290-7](https://doi.org/10.1016/S0016-7037(98)00290-7)
- Frei, R., Rosing, M. T., Waight, T. E., & Ulfsbeck, D. G. (2002). Hydrothermal-metasomatic and tectono-metamorphic processes in the Isua supracrustal belt (West Greenland): A multi-isotopic investigation of their effects on the Earth's oldest oceanic crustal sequence. *Geochimica et Cosmochimica Acta*, 66(3), 467–486. [https://doi.org/10.1016/S0016-7037\(01\)00781-5](https://doi.org/10.1016/S0016-7037(01)00781-5)
- Gardiner, N. J., Johnson, T. E., Kirkland, C. L., & Szilas, K. (2019). Modelling the hafnium-neodymium evolution of early earth: A study from West Greenland. *Journal of Petrology*, 60(1), 177–197. <https://doi.org/10.1093/ptrology/egy110>
- Gauthiez-Putallaz, L., Nutman, A., Bennett, V., & Rubatto, D. (2020). Origins of high  $\delta^{18}\text{O}$  in 3.7–3.6 Ga crust: A zircon and garnet record in Isua clastic metasedimentary rocks. *Chemical Geology*, 537, 119474. <https://doi.org/10.1016/J.CHEMGEO.2020.119474>
- Gruau, G., Rosing, M., Bridgwater, D., & Gill, R. C. O. (1996). Resetting of Sm-Nd systematics during metamorphism of >3.7-Ga rocks: Implications for isotopic models of early Earth differentiation. *Chemical Geology*, 133(1–4), 225–240. [https://doi.org/10.1016/S0009-2541\(96\)00092-7](https://doi.org/10.1016/S0009-2541(96)00092-7)
- Hayashi, M., Komiya, T., Nakamura, Y., & Maruyama, S. (2000). Archean regional metamorphism of the isua supracrustal belt, Southern West Greenland: Implications for a driving force for archaic plate tectonics. *International Geology Review*, 42(12), 1055–1115. <https://doi.org/10.1080/00206810009465128>
- Heijlen, W., Appel, P. W. U., Frezzotti, M. L., Horsewell, A., & Touret, J. L. R. (2006). Metamorphic fluid flow in the northeastern part of the 3.8–3.7 Ga Isua Greenstone Belt (SW Greenland): A re-evaluation of fluid inclusion evidence for early Archean seafloor-hydrothermal systems. *Geochimica et Cosmochimica Acta*, 70(12), 3075–3095. <https://doi.org/10.1016/j.gca.2006.04.005>
- Henry, D. J., Guidotti, C. V., & Thomson, J. A. (2005). The Ti-saturation surface for low-to-medium pressure metapelitic biotites: Implications for geothermometry and Ti-substitution mechanisms. *American Mineralogist*, 90(2–3), 316–328. <https://doi.org/10.2138/am.2005.1498>
- Hiess, J., Bennett, V. C., Nutman, A. P., & Williams, I. S. (2009). In situ U–Pb, O and Hf isotopic compositions of zircon and olivine from Eoarchean rocks, West Greenland: new insights to making old crust. *Geochimica et Cosmochimica Acta*, 73(15), 4489–4516.
- Hiess, J., Bennett, V. C., Nutman, A. P., & Williams, I. S. (2011). Archaean fluid-assisted crustal cannibalism recorded by low  $\delta^{18}\text{O}$  and negative  $\epsilon(\text{Hf}(T))$  isotopic signatures of West Greenland granite zircon. *Mineralogy and Petrology*, 101(3–4), 1027–1050. <https://doi.org/10.1007/s00410-010-0578-z>
- Hoffmann, J. E., Nagel, T. J., Münker, C., Næraa, T., & Rosing, M. T. (2014). Constraining the process of Eoarchean TTG formation in the Itsaq Gneiss Complex, southern West Greenland. *Earth and Planetary Science Letters*, 388, 374–386. <https://doi.org/10.1016/j.epsl.2013.11.050>
- Hoffmann, J. E., Zhang, C., Moyon, J.-F., & Nagel, T. J. (2019). Chapter 7 - The formation of tonalites–trondhjemite–granodiorites in early continental crust. In M. J. Van Kranendonk, V. C. Bennett, & J. E. Hoffmann (Eds.), *Earth's oldest rocks*. (edn. 2, pp. 133–168). Elsevier. <https://doi.org/10.1016/b978-0-444-63901-1.00007-1>
- Holder, R. M., Viete, D. R., Brown, M., & Johnson, T. E. (2019). Metamorphism and the evolution of plate tectonics. *Nature*, 572(7769), 378–381. <https://doi.org/10.1038/s41586-019-1462-2>
- Holland, T. J. B., & Powell, R. (2011). An improved and extended internally consistent thermodynamic dataset for phases of petrological interest, involving a new equation of state for solids. *Journal of Metamorphic Geology*, 29(3), 333–383. <https://doi.org/10.1111/j.1525-1314.2010.00923.x>
- Johnson, T. E., Brown, M., Gardiner, N. J., Kirkland, C. L., & Smithies, R. H. (2017). Earth's first stable continents did not form by subduction. *Nature*, 543(7644), 239–242. <https://doi.org/10.1038/nature21383>
- Kahl, M., Chakraborty, S., Pompilio, M., & Costa, F. (2015). Constraints on the nature and evolution of the magma plumbing system of Mt. Etna volcano (1991–2008) from a combined thermodynamic and kinetic modelling of the compositional record of minerals. *Journal of Petrology*, 56(10), 2025–2068. <https://doi.org/10.1093/ptrology/egv063>
- Komiya, T., Hayashi, M., Maruyama, S., & Yurimoto, H. (2002). Intermediate-P/T type Archean metamorphism of the Isua supracrustal belt: Implications for secular change of geothermal gradients at subduction zones and for Archean plate tectonics. *American Journal of Science*, 302(9), 806–826. <https://doi.org/10.2475/ajs.302.9.806>
- Komiya, T., Maruyama, S., Masuda, T., Nohda, S., & Okamoto, K. (1999). Plate tectonics at 3.8–3.7 Ga: Field evidence from the Isua Accretionary complex, southern West Greenland. *The Journal of Geology*, 107(5), 515–554. [https://www.journals.uchicago.edu/doi/full/10.1086/314371?casa\\_token=B5WZzTyyrK4AAAAA%3AXw53YQEXeH3KVTw8rFfEsEWrEdlUzFW8a0HBWZEPXTTuPEHGvr-J8PZ5VapCGQYFVbDMNf\\_WLYAynGKq](https://www.journals.uchicago.edu/doi/full/10.1086/314371?casa_token=B5WZzTyyrK4AAAAA%3AXw53YQEXeH3KVTw8rFfEsEWrEdlUzFW8a0HBWZEPXTTuPEHGvr-J8PZ5VapCGQYFVbDMNf_WLYAynGKq)
- Lanari, P., Vidal, O., De Andrade, V., Dubacq, B., Lewin, E., Grosch, E. G., & Schwartz, S. (2014). XMapTools: A MATLAB®-based program for electron microprobe X-ray image processing and geothermobarometry. *Computers & Geosciences*, 62, 227–240. <https://doi.org/10.1016/j.cageo.2013.08.010>
- Lenardic, A. (2018). The diversity of tectonic modes and thoughts about transitions between them. *Philosophical Transactions of the Royal Society A: Mathematical, Physical & Engineering Sciences*, 376(2132). <https://doi.org/10.1098/rsta.2017.0416>
- Miyashiro, A. (1961). Evolution of metamorphic belts. *Journal of Petrology*, 2(3), 277–311. <https://doi.org/10.1093/ptrology/2.3.277>
- Miyashiro, A. (1973). Paired and unpaired metamorphic belts. *Tectonophysics*, 17(3), 241–254. [https://doi.org/10.1016/0040-1951\(73\)90005-X](https://doi.org/10.1016/0040-1951(73)90005-X)
- Moore, W. B., & Webb, A. A. G. (2013). Heat-pipe earth. *Nature*, 501(7468), 501–505. <https://doi.org/10.1038/nature12473>
- Moyon, J. F., & Laurent, O. (2018). Archaean tectonic systems: A view from igneous rocks. *Lithos*, 302(303), 99–125. <https://doi.org/10.1016/j.lithos.2017.11.038>
- Müller, T., Dohmen, R., Becker, H. W., ter Heege, J. H., & Chakraborty, S. (2013). Fe-Mg interdiffusion rates in clinopyroxene: Experimental data and implications for Fe-Mg exchange geothermometers. *Contributions to Mineralogy and Petrology*, 166(6), 1563–1576. <https://doi.org/10.1007/s00410-013-0941-y>
- Nagel, T. J., Hoffmann, J. E., & Münker, C. (2012). Generation of Eoarchean tonalite-trondhjemite-granodiorite series from thickened mafic arc crust. *Geology*, 40(4), 375–378. <https://doi.org/10.1130/G32729.1>
- Nutman, A. P., Allaart, J. H., Bridgwater, D., Dimroth, E., & Rosing, M. (1984). Stratigraphic and geochemical evidence for the depositional environment of the early Archean Isua supracrustal belt, southern west Greenland. *Precambrian Research*, 25(4), 365–396. [https://doi.org/10.1016/0301-9268\(84\)90010-X](https://doi.org/10.1016/0301-9268(84)90010-X)

- Nutman, A. P., Bennett, V. C., & Friend, C. R. L. (2015). The emergence of the Eoarchean proto-arc: Evolution of a c. 3700 Ma convergent plate boundary at Isua, southern West Greenland. *Geological Society - Special Publications*, 389(1), 113–133. <https://doi.org/10.1144/SP389.5>
- Nutman, A. P., Bennett, V. C., Friend, C. R. L., & Chivas, A. R. (2017). Chapter 20 - The Isua supracrustal belt of the North Atlantic craton (Greenland): Spotlight on sedimentary systems with the oldest preserved sedimentary structures (~3.7, w3.75, and ~3.8 Ga). In R. Mazumder (Ed.), *Sediment provenance* (pp. 563–592). Elsevier Inc. <https://doi.org/10.1016/B978-0-12-803386-9.00020-4>
- Nutman, A. P., Bennett, V. C., Friend, C. R. L., Hidaka, H., Yi, K., Lee, S. R., & Kamiichi, T. (2013). The itsaq gneiss complex of Greenland: Episodic 3900 to 3660 Ma juvenile crust formation and recycling in the 3660 to 3600 Ma Isukasian orogeny. *American Journal of Science*, 313(9), 877–911. <https://doi.org/10.2475/09.2013.03>
- Nutman, A. P., Bennett, V. C., Friend, C. R. L., Kranendonk, M. J. V., & Chivas, A. R. (2016). Rapid emergence of life shown by discovery of 3,700-million-year-old microbial structures. *Nature*, 537(7621), 535–538. <https://doi.org/10.1038/nature19355>
- Nutman, A. P., & Friend, C. R. L. (2009). New 1:20,000 scale geological maps, synthesis and history of investigation of the Isua supracrustal belt and adjacent orthogneisses, southern West Greenland: A glimpse of Eoarchean crust formation and orogeny. *Precambrian Research*, 172(3–4), 189–211. <https://doi.org/10.1016/j.precamres.2009.03.017>
- Nutman, A. P., Friend, C. R. L., Bennett, V. C., & McGregor, V. R. (2004). Dating of the Ameralik dyke swarms of the Nuuk district, southern West Greenland; Mafic intrusion events starting from c. 3510 Ma. *Journal of the Geological Society*, 161(3), 421–430. <https://doi.org/10.1144/0016-764903-043>
- Nutman, A. P., McGregor, V. R., Friend, C. R. L., Bennett, V. C., & Kinny, P. D. (1996). The Itsaq Gneiss Complex of southern West Greenland; the world's most extensive record of early crustal evolution (3900–3600 Ma). *Precambrian Research*, 78(1–3), 1–39.
- Perchuk, L. L., & Lavrent'eva, I. V. (1983). Experimental investigation of exchange equilibria in the system cordierite-garnet-biotite. In S. K. Saxena (Ed.), *Kinetics and equilibrium in mineral reactions*. Advances in Physical Geochemistry (Vol. 3, pp. 199–239). New York, NY: Springer. [https://doi.org/10.1007/978-1-4612-5587-1\\_7](https://doi.org/10.1007/978-1-4612-5587-1_7)
- Polat, A., Hofmann, A. W., & Rosing, M. T. (2002). Boninite-like volcanic rocks in the 3.7–3.8 Ga isua greenstone belt, West Greenland: Geochemical evidence for intra-oceanic subduction zone processes in the early earth. *Chemical Geology*, 184(3–4), 231–254. [https://doi.org/10.1016/S0009-2541\(01\)00363-1](https://doi.org/10.1016/S0009-2541(01)00363-1)
- Ramírez-Salazar, A., Müller, T., Piazzolo, S., Webb, A., Hauzenberger, C., Zuo, J., et al. (2020a). *Tectonics of the Isua supracrustal belt 1: P-T-X-d constraints of a poly-metamorphic terrane. Whole rock major elements chemistry from metamorphic rocks, Version 1.0. Interdisciplinary Earth Data Alliance (IEDA)*. <https://doi.org/10.26022/IEDA/111667>
- Ramírez-Salazar, A., Müller, T., Piazzolo, S., Webb, Hauzenberger, G. A. C., Zuo, J., Haproff, P., et al. (2020b). *Tectonics of the Isua supracrustal belt 1: P-T-X-d constraints of a poly-metamorphic terrane. Garnet, biotite, plagioclase and amphibole chemistry, Version 1.0. Interdisciplinary Earth Data Alliance (IEDA)*. <https://doi.org/10.26022/IEDA/111668>
- Rollinson, H. (2002). The metamorphic history of the Isua Greenstone Belt, West Greenland. *Geological Society - Special Publications*, 199, 329–350. <https://doi.org/10.1144/GSL.SP.2002.199.01.16>
- Rollinson, H. (2003). Metamorphic history suggested by garnet-growth chronologies in the Isua Greenstone Belt, West Greenland. *Precambrian Research*, 126(3–4), 181–196. [https://doi.org/10.1016/S0301-9268\(03\)00094-9](https://doi.org/10.1016/S0301-9268(03)00094-9)
- Rosing, M. T., & Frei, R. (1999). Late Archaean metasomatism and kyanite formation in the >3700 Ma Isua supracrustals, west Greenland. In *Program and abstracts of the 10th meeting of the European Union of Geosciences (EUG)*, (Vol. 4, No. 1), Strasbourg, France: Terra Nova.
- Shen, T., Hermann, J., Zhang, L., Lü, Z., Padrón-Navarta, J. A., Xia, B., & Bader, T. (2015). UHP metamorphism documented in Ti-chondrodite- and Ti-clinohumite-bearing serpentinized ultramafic rocks from Chinese southwestern Tianshan. *Journal of Petrology*, 56(7), 1425–1458. <https://doi.org/10.1093/ptrology/egv042>
- Shimizu, H., Umemoto, N., Masuda, A., & Appel, P. W. U. (1990). Sources of iron-formations in the archaean isua and malene supracrustals, West Greenland: Evidence from La-Ce and sm-nd isotopic data and REE abundances. *Geochimica et Cosmochimica Acta*, 54(4), 1147–1154. [https://doi.org/10.1016/0016-7037\(90\)90445-Q](https://doi.org/10.1016/0016-7037(90)90445-Q)
- Sizova, E., Gerya, T., Stiwe, K., & Brown, M. (2015). Generation of felsic crust in the Archean: A geodynamic modeling perspective. *Precambrian Research*, 271, 198–224. <https://doi.org/10.1016/j.precamres.2015.10.005>
- Smit, M. A., Scherstén, A., Næraa, T., Emo, R. B., Scherer, E. E., Sprung, P., et al. (2019). Formation of Archean continental crust constrained by boron isotopes. *Geochemical Perspectives Letters*, 2019, 23–26. <https://doi.org/10.7185/geochemlet.1930>
- Smithies, R. H., Champion, D. C., & Van Kranendonk, M. J. (2009). Formation of Paleoproterozoic continental crust through infracrustal melting of enriched basalt. *Earth and Planetary Science Letters*, 281(3–4), 298–306. <https://doi.org/10.1016/j.epsl.2009.03.003>
- Spear, F. S., Kohn, M. J., Florence, F. P., & Menard, T. (1990). A model for garnet and plagioclase growth in pelitic schists: implications for thermobarometry and P-T path determinations. *Journal of Metamorphic Geology*, 8(6), 683–696.
- Turcotte, D. L. (1989). A heat pipe mechanism for volcanism and tectonics on Venus. *Journal of Geophysical Research*, 94(B3), 2779–2785. <https://doi.org/10.1029/JB094iB03p02779>
- Webb, A. A. G., Müller, T., Zuo, J., Haproff, P. J., & Ramírez-Salazar, A. (2020). A non-plate tectonic model for the Eoarchean Isua supracrustal belt. *Lithosphere*, 12(1), 166–179. <https://doi.org/10.1130/L1130.1>
- Zuo, J., Webb, A. A. G., Piazzolo, S., Wang, Q., Müller, T., Ramírez-Salazar, A., & Haproff, P. J. (2021). Tectonics of the Isua supracrustal belt 2: Microstructures reveal distributed strain in the absence of major fault structures. *Tectonics*. <https://doi.org/10.1029/2020TC006514>

## References From the Supporting Information

- Connolly, J. A. D. (2005). Computation of phase equilibria by linear programming: A tool for geodynamic modeling and its application to subduction zone decarbonation. *Earth and Planetary Science Letters*, 236(1–2), 524–541. <https://doi.org/10.1016/j.epsl.2005.04.033>
- Diener, J. F. A., & Powell, R. (2012). Revised activity-composition models for clinopyroxene and amphibole. *Journal of Metamorphic Geology*, 30(2), 131–142. <https://doi.org/10.1111/j.1525-1314.2011.00959.x>
- Green, E., Holland, T., & Powell, R. (2007). An order-disorder model for omphacitic pyroxenes in the system jadeite-diopside-hedenbergite-aemite, with applications to eclogitic rocks. *American Mineralogist*, 92(7), 1181–1189. <https://doi.org/10.2138/am.2007.2401>
- Henry, D. J., Guidotti, C. V., & Thomson, J. A. (2005). The Ti-saturation surface for low-to-medium pressure metapelitic biotites: Implications for geothermometry and Ti-substitution mechanisms. *American Mineralogist*, 90(2–3), 316–328. <https://doi.org/10.2138/am.2005.1498>
- Hoffmann, J. E., Zhang, C., Moyen, J.-F., & Nagel, T. J. (2019). The formation of tonalites–trondjemite–granodiorites in early continental crust. In *Earth's oldest rocks* (Chapter 11). <https://doi.org/10.1016/b978-0-444-63901-1.00007-1>

- Holland, T. J. B., & Powell, R. (1998). An internally consistent thermodynamic data set for phases of petrological interest. *Journal of Metamorphic Geology*, *16*(3), 309–343. <https://doi.org/10.1111/j.1525-1314.1998.00140.x>
- Holland, T. J. B., & Powell, R. (2011). An improved and extended internally consistent thermodynamic dataset for phases of petrological interest, involving a new equation of state for solids. *Journal of Metamorphic Geology*, *29*(3), 333–383. <https://doi.org/10.1111/j.1525-1314.2010.00923.x>
- Lanari, P., Vidal, O., De Andrade, V., Dubacq, B., Lewin, E., Grosch, E. G., & Schwartz, S. (2014). XMapTools: A MATLAB®-based program for electron microprobe X-ray image processing and geothermobarometry. *Computers & Geosciences*, *62*, 227–240. <https://doi.org/10.1016/j.cageo.2013.08.010>
- Leake, B. E., Woolley, A. R., Arps, C. E. S., Birch, W. D., Gilbert, M. C., Grice, J. D., et al. (1997). Nomenclature of amphiboles: Report of the subcommittee on amphiboles of the international mineralogical association, commission on new minerals and mineral names. *American Mineralogist*, *82*(9–10), 1019–1037. <https://doi.org/10.1180/minmag.1997.061.405.13>
- Locock, A. J. (2014). An Excel spreadsheet to classify chemical analyses of amphiboles following the IMA 2012 recommendations. *Computers & Geosciences*, *62*, 1–11. <https://doi.org/10.1016/j.cageo.2013.09.011>
- Newton, R. C., Charlu, T. V., & Kleppa, O. J. (1980). Thermochemistry of the high structural state plagioclases. *Geochimica et Cosmochimica Acta*, *44*(7), 933–941. [https://doi.org/10.1016/0016-7037\(80\)90283-5](https://doi.org/10.1016/0016-7037(80)90283-5)
- Nutman, A. P., Bennett, V. C., Friend, C. R. L., & Yi, K. (2020). Eoarchean contrasting ultra-high-pressure to low-pressure metamorphisms (<250 to >1000°C/GPa) explained by tectonic plate convergence in deep time. *Precambrian Research*, *344*, 105770. <https://doi.org/10.1016/j.precamres.2020.105770>
- Perchuk, L. L., & Lavrent'eva, I. V. (1983). Experimental investigation of exchange equilibria in the system cordierite-garnet-biotite. In *Kinetics and equilibrium in mineral reactions* (pp. 199–239). [https://doi.org/10.1007/978-1-4612-5587-1\\_7](https://doi.org/10.1007/978-1-4612-5587-1_7)
- White, R. W., Powell, R., Holland, T. J. B., Johnson, T. E., & Green, E. C. R. (2014). New mineral activity-composition relations for thermodynamic calculations in metapelitic systems. *Journal of Metamorphic Geology*, *32*(3), 261–286. <https://doi.org/10.1111/jmg.12071>
- White, R. W., Powell, R., Holland, T. J. B., & Worley, B. A. (2000). The effect of TiO<sub>2</sub> and Fe<sub>2</sub>O<sub>3</sub> on metapelitic assemblages at greenschist and amphibolite facies conditions: Mineral equilibria calculations in the system K<sub>2</sub>O-FeO-MgO-Al<sub>2</sub>O<sub>3</sub>-SiO<sub>2</sub>-H<sub>2</sub>O-TiO<sub>2</sub>-Fe<sub>2</sub>O<sub>3</sub>. *Journal of Metamorphic Geology*, *18*(5), 497–511. <https://doi.org/10.1046/j.1525-1314.2000.00269.x>
- Whitney, D. L., & Evans, B. W. (2010). Abbreviations for names of rock-forming minerals. *American Mineralogist*, *95*(1), 185–187. <https://doi.org/10.2138/am.2010.3371>